The Importance of Central Pacific Meridional Heat Advection to the Development of ENSO

CAIHONG WEN,[a] ARUN KUMAR,[a] MICHELLE L'HEUREUX,[a] YAN XUE,[b] AND EMILY BECKER[c]

[a] *Climate Prediction Center, NCEP/NWS/NOAA, College Park, Maryland*
[b] *Office of Science and Technology Integration, NWS/NOAA, Silver Spring, Maryland*
[c] *Rosenstiel School of Marine and Atmospheric Science/Cooperative Institute for Marine and Atmospheric Studies, University of Miami, Miami, Florida*

(Manuscript received 19 August 2020, in final form 4 April 2021)

ABSTRACT: The relationship between the warm water volume (WWV) ENSO precursor and ENSO SST weakened substantially after ~2000, coinciding with a degradation in dynamical model ENSO prediction skill. It is important to understand the drivers of the equatorial thermocline temperature variations and their linkage to ENSO onsets. In this study, a set of ocean reanalyses is employed to assess factors responsible for the variation of the equatorial Pacific Ocean thermocline during 1982–2019. Off-equatorial thermocline temperature anomalies carried equatorward by the mean meridional currents associated with Pacific tropical cells are shown to play an important role in modulating the central equatorial thermocline variations, which is rarely discussed in the literature. Further, ENSO events are delineated into two groups based on precursor mechanisms: the western equatorial Pacific type (WEP) ENSO, when the central equatorial thermocline is mainly influenced by the zonal propagation of anomalies from the western Pacific, and the off-equatorial central Pacific (OCP) ENSO, when off-equatorial central thermocline anomalies play the primary role. WWV is found to precede all WEP ENSO events by 6–9 months, while the correlation is substantially lower for OCP ENSO events. In contrast, the central tropical Pacific (CTP) precursor, which includes off-equatorial thermocline signals, has a very robust lead correlation with the OCP ENSO. Most OCP ENSO events are found to follow the same ENSO conditions, and the number of OCP ENSO events increases substantially since the start of the twenty-first century. These results highlight the importance of monitoring off-equatorial subsurface preconditions for ENSO prediction and to understand multiyear ENSO.

KEYWORDS: ENSO; Thermocline; Advection; Climate prediction; Heat budgets/fluxes; Climate variability

1. Introduction

El Niño–Southern Oscillation (ENSO) is the most important driver of climate variability on seasonal to interannual time scales (McPhaden et al. 2006). Accurate prediction of ENSO is important in anticipating its global environmental and socioeconomic impacts. McPhaden et al. (2020) recently reviewed the current progress and challenge regarding ENSO theory, predictability, and impact. In past decades, there have been significant advances in understanding the physics and predictability of ENSO. On average, dynamical models are now able to skillfully predict ENSO up to one year in advance (Jin et al. 2008). However, seasonal ENSO predictions have encountered a challenge after 2000, despite an increase in ocean observations and advances in dynamical models used for seasonal predictions (Wang et al. 2010; Barnston et al. 2012; Xue et al. 2013; Kumar et al. 2015). During this period, there were notable missed events (or false alarms) in operational dynamical seasonal forecast systems. For example, a majority of dynamical models predicted a warm event during 2012 boreal winter for forecasts initialized as late as in September 2012, while SST anomalies in the eastern equatorial Pacific abruptly reversed back to ENSO-neutral conditions (Su et al. 2014). Another example of a missed seasonal forecast was the 2017 La Niña event (L'Heureux 2018).

To improve ENSO prediction skill, it is important to understand preconditions necessary for ENSO onset. Oceanic memory associated with subsurface temperature anomalies along the equatorial thermocline has long been recognized as an important source of ENSO predictability (Zebiak 1989; Capotondi et al. 2015). Improvement in skill of dynamical model ENSO predictions has been attributed to the advent of subsurface ocean observations leading to improvements of subsurface temperature analysis, especially during the boreal spring season (Latif et al. 1998). Equatorial subsurface temperature anomalies can modulate SST variations during the subsequent summer and fall via vertical advection. Ocean preconditioning thus has the potential to assist ENSO predictions in overcoming the so-called spring predictability barrier. The importance of equatorial thermocline variations as a precursor for ENSO is supported by the coherent variations between the observed equatorial warm water volume (WWV) that precedes ENSO SST variations by 2–3 seasons (Meinen and McPhaden 2000). In addition, the strong persistence of WWV during the spring season makes it a good ENSO indicator before the spring predictability barrier (McPhaden 2003). WWV is the most widely used oceanic ENSO precursor, and is often used in statistical forecast methods for ENSO prediction, or as a diagnostic measure for the oceanic preconditions for ENSO onset (e.g., Fedorov et al. 2015; Puy et al. 2019).

Supplemental information related to this paper is available at the Journals Online website: https://doi.org/10.1175/JCLI-D-20-0648.s1.

Corresponding author: Dr. Caihong Wen, caihong.wen@noaa.gov

DOI: 10.1175/JCLI-D-20-0648.1

Physics behind the WWV–ENSO linkage are often explained by the recharge–discharge theory, which suggests that transitions between El Niño and La Niña are driven by the heat content exchange between the equatorial and off-equatorial regions via slow oceanic adjustment processes, namely Sverdrup transport (Jin 1997). However, this simple linear recharge–discharge framework faces a challenge in explaining some ENSO features, such as the short life cycle of some ENSO events, or asymmetries in the WWV and SST lead times between the two phases (i.e., longer duration of La Niña events) (Kessler 2002; Okumura and Deser 2010). The WWV/SST ENSO lead times are also documented to have decreased substantially after the late 1990s (McPhaden 2012; Horii et al. 2012). Interestingly, the breakdown of WWV/SST ENSO coincided with a degradation in ENSO prediction skill of dynamical models (Wang et al. 2010; Barnston et al. 2012; Xue et al. 2013; Kumar et al. 2015). Low-frequency temporal variations in the WWV–ENSO relationship indicates that factors other than WWV variability may also be influencing ENSO onset.

Many studies have analyzed the role of higher-frequency wind forcing in triggering ENSO onset. It is now clear that intraseasonal atmospheric impulses within the tropical Pacific associated with the Madden–Julian oscillation, westerly wind events, or easterly wind surges are important triggers for ENSO onset (e.g., McPhaden and Yu 1999; Fedorov 2002; Zhang and Gottschalck 2002; Chiodi and Harrison 2015; Lopez and Kirtman 2014; Fedorov et al. 2015; Hu and Fedorov 2016). Some studies also suggest that atmospheric fluctuations associated with extratropical teleconnections play an important role (e.g., Vimont et al. 2003; Chang et al. 2007; Alexander et al. 2010; Larson and Kirtman 2013; Hong et al. 2014; You and Furtado 2017; Luo et al. 2017). These atmospheric forcings are considered a key factor contributing to the ENSO diversity (Capotondi et al. 2015; Chen et al. 2015; Timmermann et al. 2018).

Although higher-frequency atmospheric forcings have different origins, they usually trigger ENSO events via initiating oceanic Kelvin waves along the equatorial waveguide, and hence leave their footprint in the equatorial thermocline variations. The superimposition of the role of chaotic atmosphere forcing versus the slow oceanic adjustment could lead to variations and changes in the lead time of ENSO predictability associated with WWV. Using a wind-forced ocean model, Neske and McGregor (2018) demonstrated that the decadal changes in the relative importance of the instantaneous wind response versus slow oceanic adjustment processes led to a reduction in WWV/SST ENSO lead time from 6 to 9 months in the pre-2000 period to three months during the post-2000 period. Meinen and McPhaden (2000) suggested that western equatorial (WE) Pacific thermocline variations, which are a better integral measure of slow ocean adjustment, have a stronger relationship with ENSO at longer time leads (~10 months) than WWV. Using a longer record of observations and CMIP5 models, Izumo et al. (2019) confirmed that the content in the WE Pacific is a better precursor prior the spring predictability barrier. Zonal advection by the equatorial undercurrent could also play an important role in connecting the western Pacific thermocline variations with those in the central equatorial (CE) Pacific that are associated with ENSO (Ballester et al. 2016; Lu et al. 2017). Although pointing to different mechanisms, all these studies nevertheless focus on the contribution of equatorial waves related subsurface thermal variations on the CE thermocline variability.

In addition to equatorial processes, subtropical water mass transport also can modulate the equatorial thermocline variation via oceanic pathways. Subtropical cells (STCs) are an important pathway connecting the subtropics with the equator (e.g., Kleeman et al. 1999; McPhaden and Zhang 2002; Farneti et al. 2014). The impact of subtropical water mass transport on ENSO is often discussed on decadal time scales, because it usually takes years for subtropical signals to be advected to the equator. Recently, some studies indicated that off-equatorial (OE) subsurface signals could modulate equatorial thermocline variations on seasonal time scales. Using numerical model experiments, Zhang et al. (2013) showed that the persistent negative subsurface anomaly in the central tropical Pacific during boreal spring 2011 was an important factor causing the onset of La Niña later in 2011. Wen et al. (2014) found that thermocline variations averaged in the central tropical Pacific (CTP) during the early summer season were crucial for ENSO events when WWV failed as a predictor. Their analysis also indicated that the difference between CTP and WWV events depended on the preconditioning in the off-equatorial region. Although indicative, these studies did not provide an in-depth analysis of the dynamical processes contributing to the linkage between off-equatorial and equatorial thermocline variations on a seasonal time scale.

In this study, we use a set of ocean reanalysis products to further examine the predictability of two oceanic precursor indices, WWV and CTP, for all ENSO events during 1982–2019. We focus on addressing the following questions: What is the predictive potential of these two precursors for ENSO onset with 6–7-month lead? What are the physical mechanisms leading to differences in predictive potential between CTP and WWV? Are such differences related to a specific precursor-driven type of ENSO? How do the off-equatorial thermocline anomalies influence the equatorial thermocline variations? Answers to these questions will shed light on the dynamics and predictability of ENSO and help explain possible reasons for the decrease in dynamical model prediction skill in recent decades.

The rest of the paper is organized as follows. A brief description of the datasets and methods to quantify the two oceanic precursors is presented in section 2. In section 3, skill of the two precursors in predicting ENSO is quantified. In section 4, the differing skills of the two precursors are linked to the relative importance of off-equatorial preconditions versus the equatorial wave related preconditions on the central equatorial thermocline variations. Based on the two precursor-driven mechanisms, ENSO events are classified into two groups: the western equatorial Pacific–driven ENSO (WEP), when the central equatorial thermocline is mainly influenced by the zonal propagation of anomalies from the western Pacific; and the off-equatorial central Pacific–driven ENSO (OCP), when off-equatorial central thermocline anomalies play the primary role. The characteristics of the two type ENSO are further described in section 4. In section 5, we study

the relative importance of advective processes in modulating the CE thermocline variations. In particular, we explore how the OE subsurface anomalies affect the equatorial thermocline temperature tendency. Last, conclusions and discussion of the implications of our findings in understanding variations in dynamical model ENSO predictability and ENSO theories are presented in section 6.

2. Data and methods

Depth of the 20°C isotherm (D20) is a proxy measurement of the thermocline layer depth. The monthly D20 data were obtained from the Real-Time Ocean Reanalysis Intercomparison Project, which has collected an ensemble of six operational ocean reanalysis products (ORAs) from 1979 to the present (Xue et al. 2017). The ensemble includes NCEP GODAS (Behringer and Xue 2004), ECMWF Ocean Reanalysis system 5 (Zuo et al. 2018), JMA MOVE/MRI.COM-G2 (Toyoda et al. 2013), GFDL ECDA (Zhang et al. 2007), NASA MERRA Ocean (Vernieres et al. 2012), and BOM POAMA (Yin et al. 2011). Readers are referred to Xue et al. (2017) for further details about the ORAs. The ensemble data are available from 1979 to present. Xue et al. (2017) found that the ensemble mean is a more accurate representation of ocean variability than individual ORAs. Therefore, the ensemble mean of D20 anomaly is used to represent the best estimation of the ocean state. Uncertainty (or the noise) among ocean reanalysis products is quantified as departures in individual analysis from the ensemble mean. The robust features among the ORAs are quantified by the ratio of ensemble mean signal and the noise.

In this study, we focus on examining two oceanic ENSO precursors: WWV and CTP. The WWV index is calculated as an average of the D20 anomaly across the equatorial Pacific (120°E–80°W, 5°S–5°N) (Meinen and McPhaden 2000). The CTP index is defined as the averaged D20 anomaly in the central tropical Pacific (160°–110°W, 10°S–10°N) (Wen et al. 2014). We also examine two other oceanic indices, the eastern Pacific heat content precursor (WWVE; D20 averaged over 155°–80°W, 5°S–5°N) and Niño-3.4 SST, which are good predictors for the upcoming El Niño after the spring predictability barrier (Planton et al. 2018; Izumo et al. 2019).

To provide a baseline for forecast skill comparison of the two precursors, we develop two separate univariate regression models using either the CTP and WWV as predictors and the boreal wintertime [November–January (NDJ)] Niño-3.4 index as the predictand. The models are cross-validated in two ways: 1) using leave-one-year-out cross-validation over the full period by iteratively recomputing the coefficients with the target prediction year removed, and 2) building the models on half of the historical period (training data) and testing the skill on the other remaining half (test data). These two statistical models are then used for determining whether the WWV or CTP provides more skill. The significance of the comparison is determined using a sign test, which evaluates which model makes a ''better'' forecast of a particular event (Diebold and Mariano 1995). The null hypothesis is that if two models are equally skillful then the probability that one beats the other is 50% (e.g., a fair coin with heads and tails). The null hypothesis is rejected if the number of heads falls outside of the 95% interval computed from a binomial distribution. To illustrate the results of the sign test, the random walk diagram of DelSole and Tippett (2016) is employed. The random walk is indicated by a step in the positive or negative direction depending on whether the error (forecast minus observed) of one prediction model is smaller or larger than the error of the other model. The 95% significance bounds are indicated by a gray cone and deviations beyond this cone indicate that one forecast model is providing statistically significant skill beyond the other forecast model.

To explore the linkage between the degraded ENSO skill of dynamical model in recent decades with the ENSO types identified in section 4, we use the SST predictions from an ensemble of seven seasonal prediction systems from the North American Multi-Model Ensemble (NMME) project (Kirtman et al. 2014). At the time the initial analysis was completed, the operational NMME included the CanCM4i, GEM_NEMO, CFSv2, GFDL, GFDL_FLOR, NCAR_CCSM4, and NASA_GEOS5v2 models. Readers are referred to the Climate Prediction Center (CPC) website (https://www.cpc.ncep.noaa.gov/products/NMME/) and Becker et al. (2020) for more details. The dataset spans the period from January1982 to the present.

The SST in Niño-3.4 region (170°–120°W, 5°S–5°N) from OISST data (Reynolds et al. 2002) is used to represent ENSO status. The Niño-3.4 index was downloaded from NOAA CPC (https://www.cpc.ncep.noaa.gov/data/indices/sstoi.indices). Following the National Oceanic and Atmospheric Administration's (NOAA's) ENSO definitions, warm (cold) events are defined when Niño-3.4 SST anomalies are higher (lower) than 0.5°C (−0.5°C) for a minimum of five consecutive overlapping seasons. Using this criterion, there are 13 El Niño years (1982, 1986, 1987, 1991, 1994, 1997, 2002, 2004, 2006, 2009, 2014, 2015, 2018), 13 La Niña years (1983, 1984, 1988, 1995, 1998, 1999, 2000, 2007, 2008, 2010, 2011, 2016, 2017), and 12 neutral years within our analysis period (1982–2019).

The monthly ocean temperature and current data from the NCEP Global Ocean Data Assimilation System (GODAS) (Behringer and Xue 2004) is used for heat budget analysis. GODAS is based on the GFDL MOM.v3 model, which is driven by surface fluxes derived from the NCEP R2 atmospheric reanalysis (Kanamitsu et al. 2002). Observed temperature and synthetic salinity profiles are assimilated into the model with a 3D variational (3DVAR) data assimilation scheme. The native GODAS data are available at a 1° × 1/3° horizontal resolution in the tropics and has 40 vertical levels with 10-m resolution near the sea surface. The monthly mean fields with resolution on a 1° × 1° horizontal grid are used in this study. The data are available from January 1979 to the present.

We also compared the D20–SST ENSO relationship with two other variables: surface zonal wind and surface zonal current, which are also important for ENSO development (e.g., Capotondi et al. 2015; Wang et al. 2017; Timmermann et al. 2018). The monthly 10-m zonal winds were obtained from ERA-Interim atmospheric reanalysis (Dee et al. 2011), with data available from January1979 to August 2019. The monthly surface current analysis from Ocean Surface Current Analysis–Real Time (OSCAR) (Bonjean and Lagerloef 2002) was

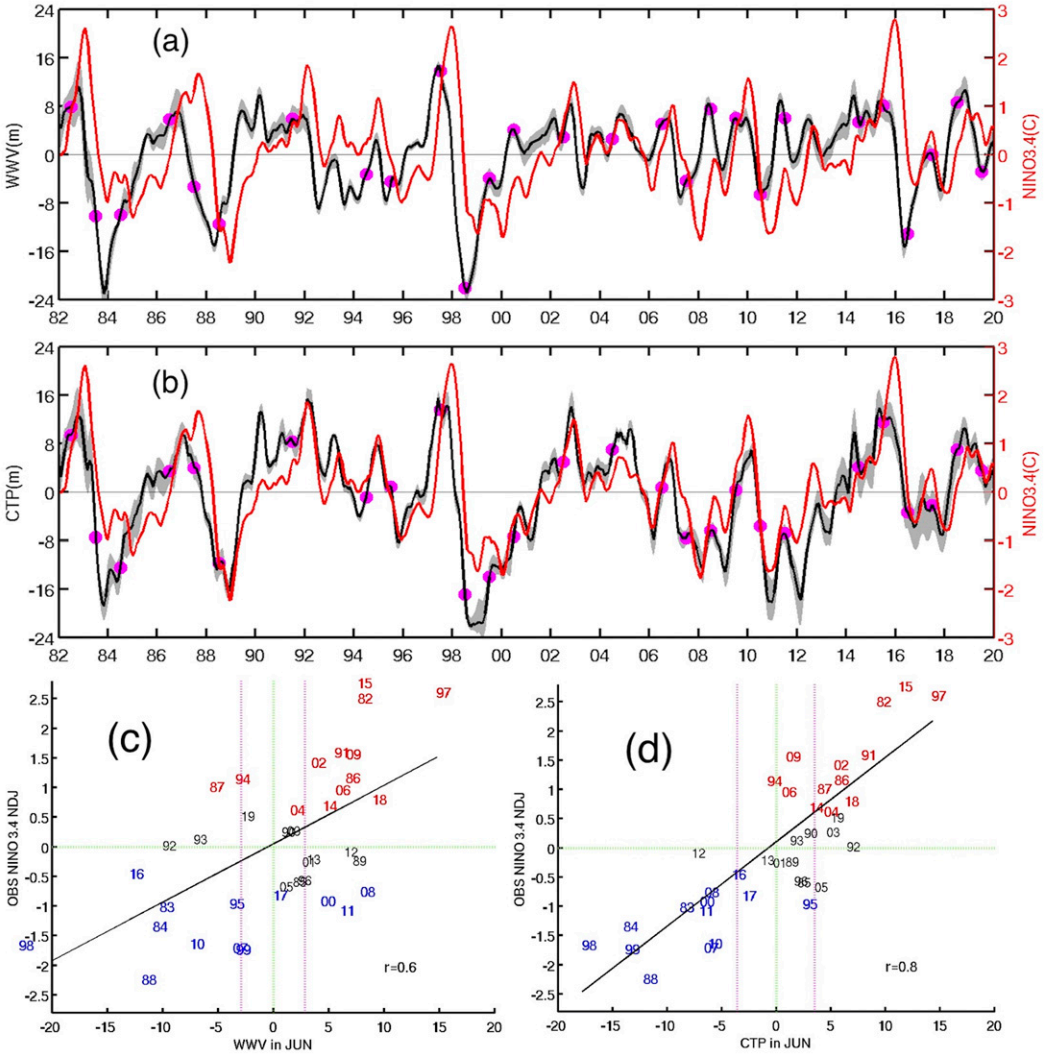

FIG. 1. Time series of (a) WWV (black line), defined as the ensemble mean D20 anomaly (m) averaged over 5°S–5°N, 120°E–80°W and (b) CTP (black line), defined as the ensemble mean D20 anomaly averaged over 10°S–10°N, 160°–110°W. In (a) and (b) shading denotes the maximum and minimum of the six ocean reanalysis products, and the red lines display the observed Niño-3.4 anomaly. Purple dots mark the value of WWV or CTP in June during the ENSO development. (c) Scatterplot of WWV (m) in June and observed Niño-3.4 indices in November–January (NDJ; °C) during 1982–2019. The numerals denote the last two digits of the year (e.g., for NDJ "97" means November 1997–January 1998). The red, blue, and black text colors represent El Niño, La Niña, and ENSO neutral years, respectively; *r* is the correlation coefficient. The purple lines denote threshold value of WWV to qualify an ENSO year projection. (d) As in (c), but for the CTP.

obtained from ftp://ftp.esr.org. The data span from October 1992 to the present.

For the GODAS data and ERA-Interim winds, anomalies were defined as departures from the 1981–2010 monthly climatology. OSCAR current anomalies refer to the 1993–2017 climatology. The NMME forecast anomalies are formed by removing the lead-dependent monthly means from 1982 to 2010. The anomalies presented in the following sections were not detrended, but the results and conclusions are the same using detrended data.

3. Oceanic precursors and connection of thermocline variations with ENSO onset

a. Relationship between precursors and ENSO

Figures 1a and 1b show that WWV variations precede the Niño-3.4 index by about 6–9 months before the late 1990s, while the correlation breakdown afterward, consistent with previous findings (McPhaden 2012; Horii et al. 2012). In contrast, the CTP index more clearly leads ENSO by several months both before and after the late 1990s. Scatterplots in

Figs. 1c and 1d also show the relationship between the precursors in June and the Niño-3.4 index for NDJ season. There is a nearly linear relationship between ENSO and the WWV and CTP indices, confirming the importance of ocean preconditioning on ENSO onset proposed in the literature (Ren and Jin 2013).

The purple lines in Figs. 1c and 1d provide thresholds for WWV and CTP values that are greater or less than 40% of their own standard deviation. If a precursor is above (below) than a threshold value, an El Niño (La Niña) event is expected. Using these vertical lines as a visual guide, it is evident that the WWV_{JUN} anomalies are linked to the onset of 19 ENSO events. However, large positive WWV values were associated with the subsequent development of La Niña in three years (2000, 2008, 2011), which according to the recharge theory, should evolve into El Niño condition. Also, a negative WWV index value in June 1987 was followed by an El Niño event, which is surprising given the strong discharged state. In contrast to WWV, CTP_{JUN} preceded 21 ENSO events, whereas in no cases did a negative CTP value precede El Niño, nor did a positive CTP value precede La Niña. As expected from the tighter relation between CTP and ENSO, the correlation coefficient is 0.8 between the indices, whereas the correlation between WWV and Niño-3.4 is 0.6. Note that both correlation coefficients are statistically significant.

To assess whether the CTP index may offer greater predictive skill of ENSO than the WWV index, two univariate regression models are compared using the respective indices. Figure 2a shows the model comparison based on leave-one-year-out cross-validation, across the full period of 1982–2019. The gray cone maps out the 95% range of uncertainty, which means that the CTP-based model, in the recent record beyond 2010, is emerging from the cone and more skillfully predicts ENSO than the WWV-based model, particularly for forecasts based on CTP from the months of June and August. Figures 2b and 2c display the random walk diagrams tested on the first half of the period (1982–99) versus the second half of the period (2000–19). Splitting the data results in smaller sample sizes to estimate the regression coefficients, but nevertheless Fig. 2c shows that coefficients created from the first half of the record and tested on the 2000–19 period suggest that the CTP-based model is performing better than the WWV-based model. For the test period of 1982–99, neither model appears to be more skillful than the other, although it is evident there are more steps taken in the positive direction—just not so many that the null hypothesis of equal skill can be rejected. Overall, it appears the CTP index, particularly during June and August, became an important predictor of subsequent ENSO development than the WWV after 1999.

Recent studies suggested that WWVE precursor or the typical ENSO indices such as Niño-3.4 index can beat WWV after the spring predictability barrier (Planton et al. 2018; Izumo et al. 2019) because these indices record clear equatorial Kelvin waves in response to wind anomalies in the central Pacific. One might question whether these two precursors are able to project those ENSO events at which the WWV fails while the CTP succeeds. Figure 3 displays the time series of

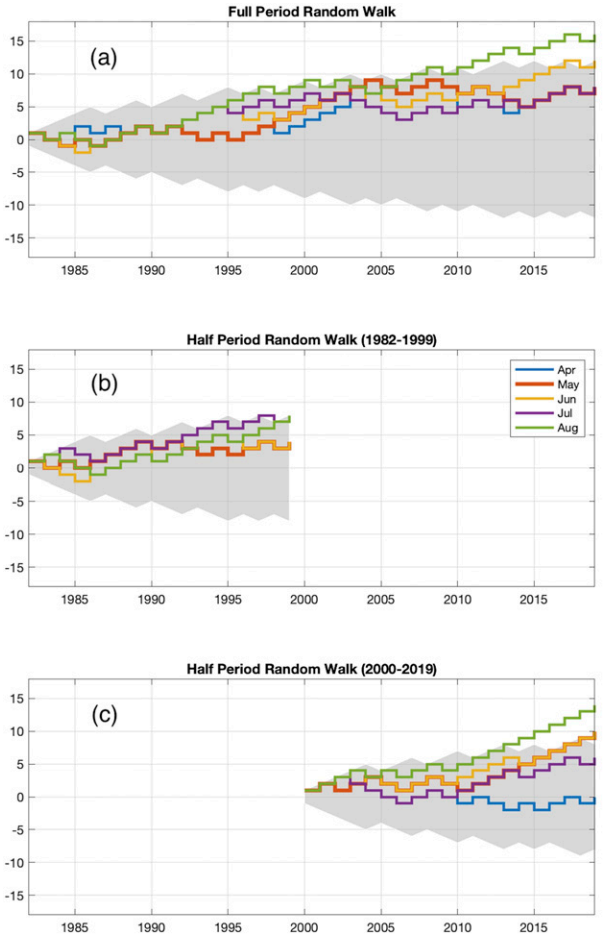

FIG. 2. Random walk diagrams applied to three different regression model configurations: (a) leave-one-out-cross-validation over the full period, 1982–2019; (b) coefficients computed from the second half of the period and tested on 1982–99; and (c) coefficients computed from the first half of the period and tested on 2000–19. Steps taken in the positive direction indicate that the model using CTP as a predictor to forecast the November–January (NDJ) Niño-3.4 value has lower error than the model using WWV as a predictor. Lines indicate the month of the CTP/WWV predictor index, which precedes the NDJ Niño-3.4 index. The gray shaded region shows the 95% significant bounds.

NDJ Niño-3.4 predictions from the four precursors: WWV, WWVE, CTP, and Niño-3.4 in June. Except for the Niño-3.4 precursors, the other three prediction models are constructed using the univariate regression model across the whole period. Although WWVE and Niño-3.4 have similar prediction skills to the CTP in terms of correlation and root-mean-square measurements, both WWVE and Niño-3.4 prediction miss the 2004 El Niño and 2008, 2011, and 2017 La Niña years, when WWV also fails. This indicates that preconditions associated with equatorial wave processes alone (slow oceanic adjustment and fast ocean Kelvin waves) could not explain the onset of these ENSO events. It is important to understand why CTP preconditions can accurately project these events.

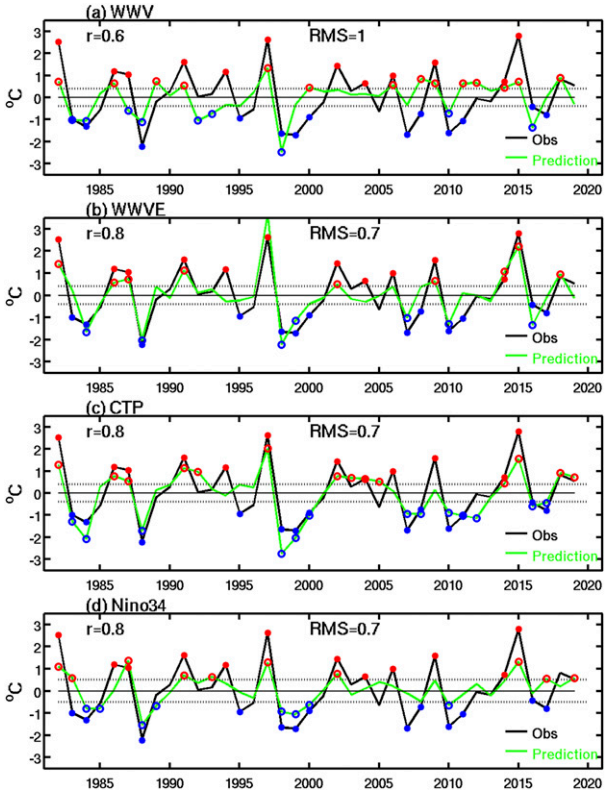

FIG. 3. Time series of predicted Niño-3.4 in NDJ season using (a) June WWV, (b) June WWVE (155°–80°W, 5°S–5°N), (c) June CTP, and (d) June Niño-3.4 as predictors (green lines). For the WWV, WWVE, and CTP precursors, prediction models are constructed using leave-one-year-out cross-validation over the full period by iteratively recomputing the coefficients with the target prediction year removed. Persistent June Niño-3.4 are considered as the predicted Niño-3.4 in NDJ. Black lines are the observed NDJ Niño-3.4 values. Red and blue dots represent the observed El Niño and the La Niña events, respectively. Red and blue circles represent the predicted El Niño and the La Niña events, respectively. Here r denotes the correlation between the predicted NDJ Niño-3.4 and the observed NDJ Niño-3.4; RMS denotes the root-mean-square error between the prediction and the observation.

b. *Physical basis for predictability*

To better understand why CTP appears to offer more skill than WWV, especially during the later period, the physical basis for their predictability is explored. Previous studies suggested slow oceanic adjustment associated with the recharge/discharge paradigm, zonal propagation of oceanic Kelvin waves, and off-equatorial (OE) thermocline variability are potentially important mechanisms in the equatorial Pacific Ocean. Not only does the CTP become increasingly important after 1999, but the period starting in 2000 corresponds to an overall decadal shift in ENSO characteristics and prediction skill (e.g., Lee and McPhaden 2010; Wang et al. 2010; Hu et al. 2020). With increasing occurrence of the central Pacific or "Modoki" El Niño after 2000 (Ashok et al. 2007), some studies suggest that zonal advection has played an increasingly important role in the development of ENSO, while the thermocline feedback has played a secondary role (e.g., Yu et al. 2010; Kug et al. 2010). To understand how these factors work together, we next examined their evolutions focusing on the ENSO events during 1998–2019.

The Hovmöller diagrams shown in Figs. 4 and 5 show that the central equatorial (CE) D20 anomaly between 160° and 110°W leads ENSO onset (black lines) by several months for all ENSO events. It confirms the important role of subsurface conditions in ENSO onset. This is consistent with analysis by Wen et al. (2014). The event-by-event examination also suggests that ENSO events can be categorized into two groups based on their spatial and temporal connection between CE D20 anomalies and surrounding areas (WE and OE regions).

For cases when the western Pacific origin is more evident, the common feature is a clear eastward propagation of D20 anomalies from the western to the CE Pacific. There is clear evidence that slow oceanic adjustment plays an important role in modulating the CE thermocline variation for some ENSO events. For example, a negative D20 anomaly accumulated in the western Pacific during summer 1997 (Fig. 4), when westerly wind anomalies and strong positive zonal current anomalies prevailed across the equatorial regions. The eastward propagation of negative D20 anomalies along the equator eventually reversed the 1997 El Niño to a La Niña. These evolutions are consistent with the recharge/discharge paradigm. A set of strong easterly wind surges developed during the decay of the 1997/98 El Niño, giving rise to the amplification of negative D20 anomalies and negative surface zonal current anomalies along the equator. These factors further enhanced the SST cooling tendency during the 1998 La Niña development. The important role of WE Pacific preconditions on ENSO onset is also evident in some other events, like the La Niña onsets in 2007, 2010, and 2016, and the 2006, 2009, and 2014 El Niño onsets.

For the other cases when the OE region connection is more important, there is no clear indication of the eastward propagation of D20 anomalies from the WE Pacific to the central Pacific prior to onset. For example, during April–June 2008 (Fig. 5, green box), positive equatorial D20 anomalies were present along the equator and large positive surface zonal current anomalies prevailed in the central-eastern Pacific (Fig. 5). These conditions indicated that the 2007 La Niña might transition to ENSO neutral or El Niño. Instead, negative D20 anomalies re-emerged in the CE region (160°–110°W) during the summer, reversing the warming trend in SST. The subsequent enhancement of the trade winds and negative zonal current anomalies further cooled the SSTs, resulting in another La Niña. The persistently large negative OE D20 anomalies (Fig. 5d) appear to be the only candidate leading to the re-emergence of negative equatorial D20 anomaly during the summer of 2008. The importance of OE thermocline variations is also evident for the formation of La Niña in 1999, 2000, 2011, and 2017 and for El Niño formation in 2002 and 2004. Note that weaker OE thermocline anomalies during 2017 occur because of large uncertainty among the multiple ocean reanalysis products at this period (Fig. 1b). Four members have strong negative OE anomalies, while a

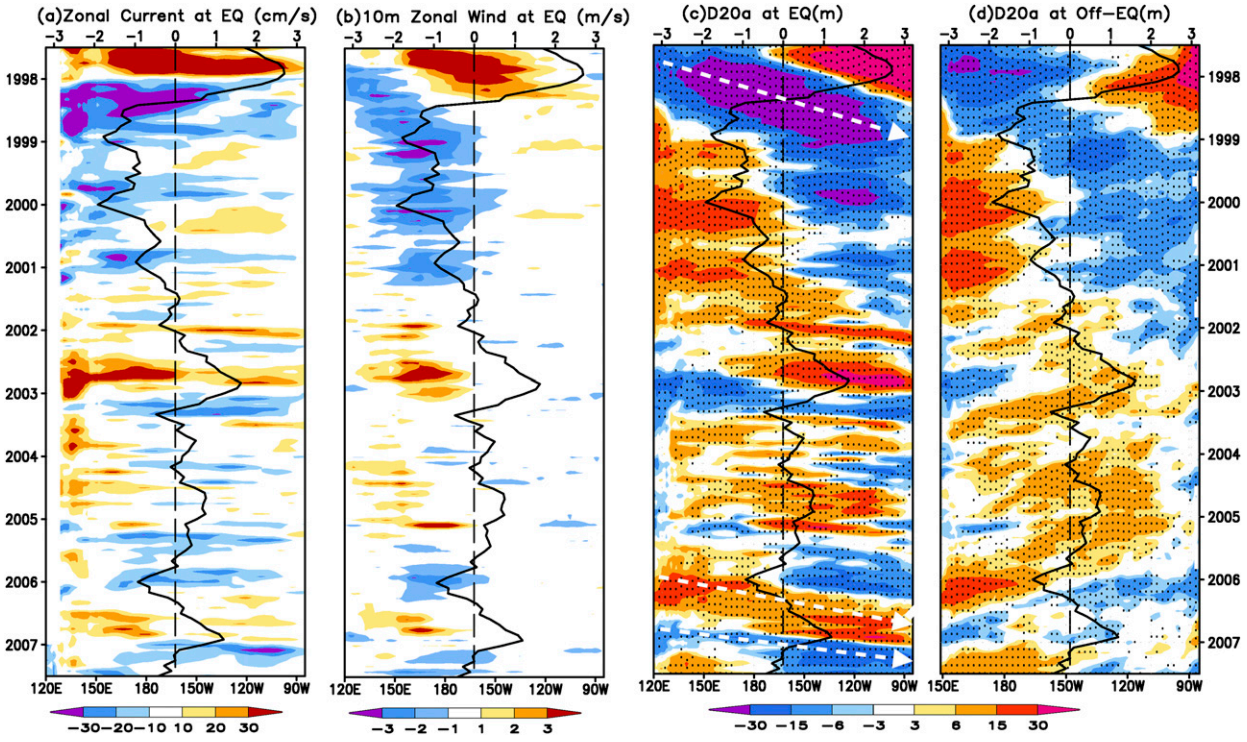

FIG. 4. Time–longitude diagram of monthly (a) surface zonal current (cm s^{-1}) from OSCAR averaged over 5°S–5°N, (b) 10-m zonal wind (m s^{-1}) from ERA-Interim averaged over 5°S–5°N, (c) D20 anomaly (m) averaged over 2°S–2°N, and (d) D20 anomaly (m) averaged in off-equatorial regions (10°–5°S and 5°–10°N) during 1997–2007. In (c) and (d), shading denotes the ensemble mean of six ocean reanalysis products, and the dotted area represents regions where the signal-to-noise ratio is greater than 1. The black contour in each panel denotes the observed Niño-3.4 anomaly (°C) from OISST. Arrows indicate the eastward propagations of D20 anomalies from the western to the central equatorial Pacific.

couple of members have very weak signals leading to the weaker ensemble mean signals.

Figures 4 and 5 suggest that D20 anomalies in the CE are connected with the western Pacific and the off-equatorial regions. It is conceivable that differences in the prediction skills of the two precursors might be related to two groupings of ENSO: one has a stronger relationship with WWV (representing the equatorial thermocline variation) while the other is related to CTP (which also includes off-equatorial thermocline variations). To explore this possibility, we track the spatial connection of D20 signals in the CE Pacific with surrounding regions. The off-equatorial region is defined as the D20 anomaly averaged over the region 160°–110°W, 5°–10°N/10°–5°S [referred to as the off-equatorial central Pacific index (OCPI)], following Wen et al.'s (2014) definition. The CE region is defined as 160°–110°W, 2°S–2°N [referred as to as the CEP index (CEPI)], which has the same zonal band as the CTP. The thermocline region west of the CEP [160°E–160°W, 2°S–2°N, referred as the WEP index (WEPI)] is used to represent variability in the western equatorial Pacific. To distinguish the two types, we use a simple metric that compares the strength of WEPI and OCPI during March–May, with CEPI during July–September. If WEPI is in the same phase as CEPI and its magnitude is greater than OCPI, then a western equatorial Pacific (WEP)-type ENSO is defined. On the other hand, if OCPI is in the same phase as CEPI, with a magnitude greater than WEPI, then an off-equatorial central Pacific (OCP)-type ENSO is defined.

Except for 1994 (weak El Niño), 25 out of 26 ENSO events can be categorized as either WEP (15 events) or OCP (10 events) (Fig. 6). The ENSO event categorization (Table 1) also illustrates that the prediction skill of WWV and CTP indices are highly dependent on ENSO type. WWV_{JUN} is a very good predictor for the WEP-type ENSO, which is evident in the 100% hit rate (15/15) and 0.9 correlation coefficient ($p > 0.99$) between WWV_{JUN} and $NINO34_{NDJ}$ with 6-month lead. In addition, WWV can predict most WEP-type ENSO events (except for 2006 and 2009 El Niño and 2010 La Niña) with 9-month lead (Fig. 7b). However, WWV_{JUN} fails to predict six OCP ENSO and the correlation coefficient drops to 0.3, which is not statistically significant ($p = 0.5$). In contrast, CTP_{JUN} successfully predicts nine OCP ENSO events, but not the 2017 La Niña, which can be attributed to the large uncertainty among the reanalysis datasets (Fig. 1b). In addition, for the El Niño projection, the false alarm rate (false alarms divided by the total number of event forecasts) of the WWV (7 out of 17) is higher than that of CTP (4 out of 14). For the La Niña projection, the false alarm rate for WWV (4 out of 13) is about 4

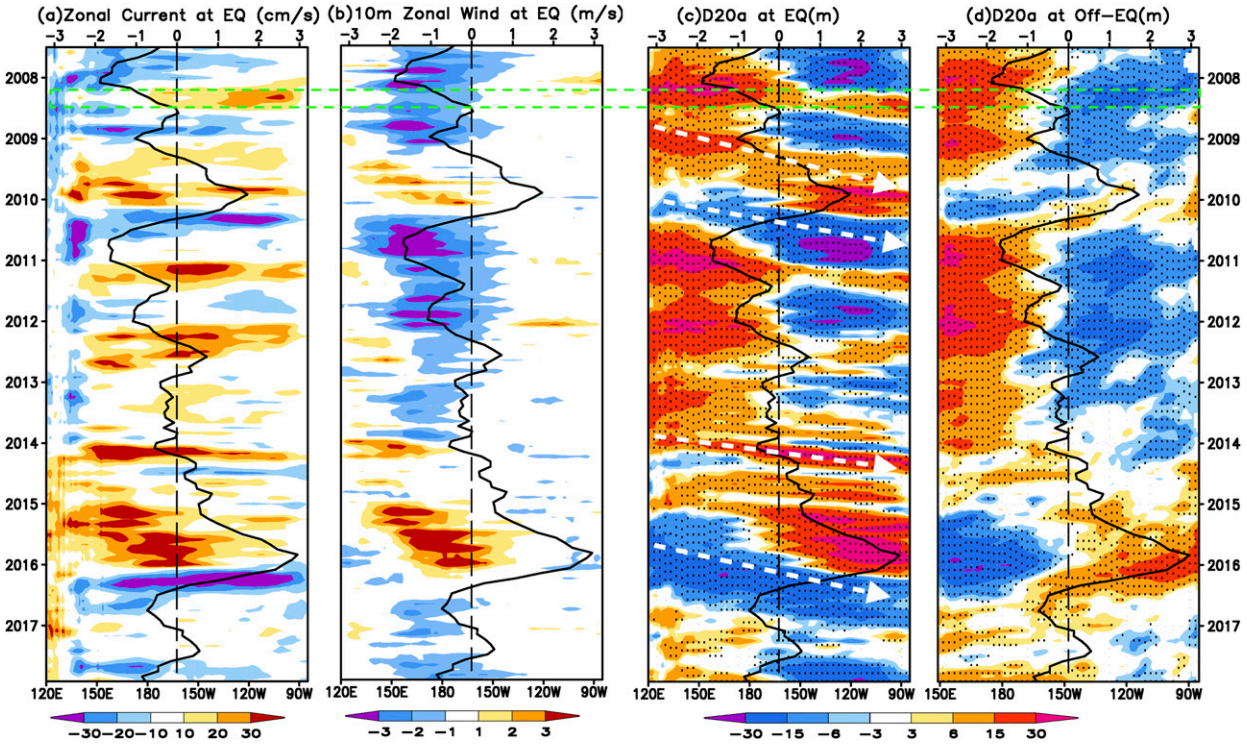

FIG. 5. As in Fig. 4, but for the 2007–17 period. The green box marks the time period of April–June 2008 discussed in the text.

times higher than that for the CTP (1 out of 12) (Figs. 1c,d). The dependence of precursor skills on the two ENSO type is also visualized in scatterplots Figs. 7a–c. This suggests that WWV is important for the WEP ENSO but is not a sufficient indicator for the onset of OCP ENSOs. The high skill of CTP for OCP ENSO highlights the crucial role of OE thermocline conditions on ENSO onset.

It is noteworthy that the number of OCP ENSO after the late 1990s is 4 times of that before the late 1990s (a total of 8 compared to 2), indicating that the OCP ENSO is more active since 1999. In contrast, the frequency of the WEP ENSO is similar before and after the late 1990s. It suggests that the increased frequency of OCP ENSO since the late 1990s contributed to the breakdown of the lead–lag WWV–ENSO relationship reported in the previous studies. Both WWV_{JUN} and CTP_{JUN} fail to predict 1994 El Niño, indicating that the onset of the 1994 warm event had little relationship with subsurface conditions. Other processes, such as thermodynamics involving the wind–evaporation–SST feedback, might have played a more important role (e.g., Vimont et al. 2003; Chang et al. 2007; Alexander et al. 2010).

4. Characteristics of two types of dynamically distinguished ENSO

To illustrate further the distinct characteristics of the two precursor mechanisms, we analyzed the composite evolution of ENSO events classified as OCP and WEP types. Figure 8 displays D20 anomaly composites. For the WEP type, during ENSO onset in May–July [MJJ(0)] the warm and cold phases have a clear basinwide pattern stretching along the equator. During the development and mature phases of ENSO, an east–northwest seesaw dipole forms with centers of action in the eastern equatorial Pacific and to the east of the Philippines (from the equator to 15°N) and leads to the ENSO phase transition. The key role of equatorial thermocline anomalies in modulating ENSO is further manifested in the evolution of subsurface temperature along the equator (Figs. 9a–d, i–l). The evolution of the subsurface pattern associated with the WEP type is in line with the recharge/discharge and the delayed oscillator mechanisms (Jin 1997; Suarez and Schopf 1988; Battisti and Hirst 1989).

The evolution of the OCP composite has salient differences from the WEP precursor in that a relatively stationary dipole pattern, with centers of action in the western and eastern equatorial Pacific Ocean, is apparent during the entire ENSO evolution cycle. For example, before the onset of OCP La Niña [FMA(0)], positive (negative) D20 anomalies exist in the western (central-eastern) equatorial Pacific (Fig. 8m). Because all the OCP La Niña events are La Niñas that persist beyond the first year (Table 1), the February–April [FMA(0)] composite actually represents the decay phase of WEP type La Niña. Negative D20 anomalies in the central-eastern Pacific decay to neutral in MJJ(0) and then reemerge in August–October [ASO(0)] without discernible eastward propagation. Also, there is no connection between the temperature anomalies

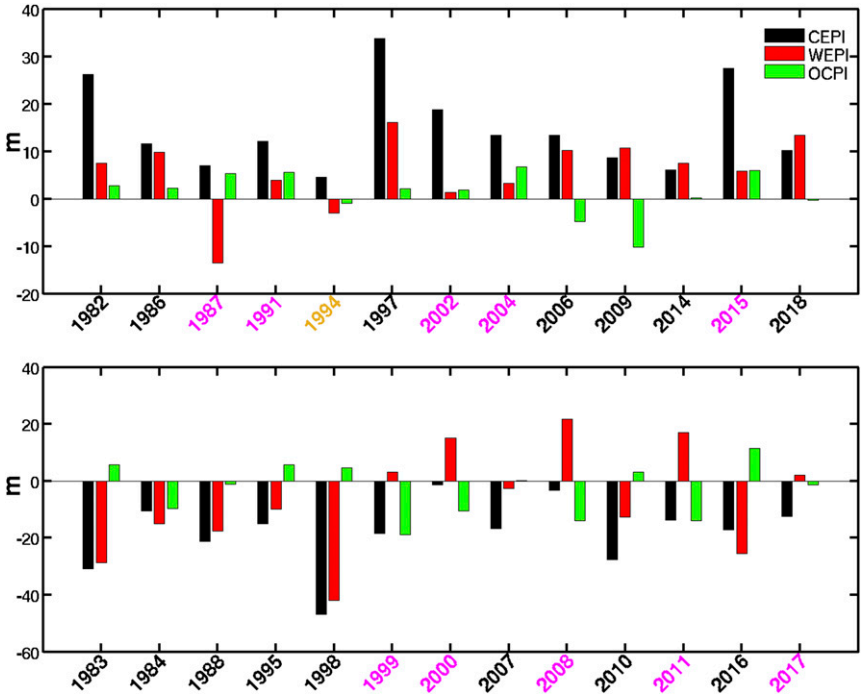

FIG. 6. Comparisons of CEPI in July–September (black bars) defined as the D20 anomaly average over 160°–110°W, 2°S–2°N, WEPI in March–May (MAM; red bars) defined as the D20 anomaly averaged in the western-equatorial region (160°E–160°W, 2°S–2°N), and OCPI in MAM (green bars) defined as the D20 anomaly average over 160°–110°W, 5°–10°N/10°–5°S for (top) El Niño events and (bottom) La Niña events. If WEPI is in the same phase as CEPI and |WEPI| > |OCPI|, then a western equatorial Pacific (WEP) ENSO (years in black text) is defined. If OCPI is in the same phase as CEPI and |OCPI| > |WEPI|, then an off-equatorial central Pacific (OCP) ENSO (years in magenta text) is defined. The year 1994 is neither WEP ENSO or OCP ENSO. Historical events of the two types of ENSO are listed in Table 1.

near the thermocline and the surface temperature anomalies during MJJ(0) (Figs. 8n and 9n). This suggests that the source of the subsequent enhancement of negative temperature in the central Pacific near the thermocline during ASO(0) is not from the overlying surface or from the western Pacific (Fig. 9o). Thus, it supports the hypothesis that the CE thermocline variations preceding ENSO for OCP-type events are associated with the OE subsurface anomalies. For the OCP El Niño composites, we have two El Niño events (1987 and 2015) that persist beyond the first El Niño year and three events (1991, 2002, and 2004) preceded by an ENSO neutral year. There is a large variance in the timing of these OCP El Niño onsets (Fig. S1 in the online supplemental material). Signals exceeding the 90% significance level are mainly confined at the OE regions during FMA(0) (Fig. 8e). The CE D20 anomaly weakens during spring season and then re-intensifies rapidly during late spring/summer. Similar to the OCP La Niña, significant signals persist in the OE regions during FMA(0)–NDJ(0). We note that in Fig. 9, both the mixed layer depth and D20 are taken as the annual mean from GODAS. The mixed layer depth is defined as the depth where the density difference from the surface is 0.125 kg m^{-3} (Levitus 1982).

We further examined whether subsurface current anomalies associated with the two types exhibit distinct features. Similar to Wen et al. (2014), the thermocline currents are defined as the vertically integrated current from the mixed layer depth to the D20 that are shown in Fig. 10. For the WEP type, equatorward meridional current anomalies are observed in the central-eastern Pacific during FMA(0) (Fig. 10a). With the development of El Niño (reverse the direction for La Niña), the equatorward convergence decays in the central Pacific while the poleward meridional current anomalies are enhanced west of 170°W and subsequently dominate the whole equatorial basin at the peak of El Niño [NDJ(0)]. This is consistent with the recharge/discharge paradigm, in which the equatorial heat content is rapidly discharged after the peak of El Niño by the poleward meridional mass transport.

Figure 10 also shows that notable zonal current anomalies are observed during the ENSO cycle. In the WEP composites, strong positive zonal current anomalies accompanied the enhanced meridional current convergence in the central-eastern Pacific during FMA(0), whereas strong negative current anomalies were present during NDJ(0). This is consistent with the enhanced meridional divergence. The magnitude of the ENSO-related zonal current anomaly is about 20 cm s^{-1} in the

TABLE 1. All observed El Niño years (first column), their types (second column), and the El Niño condition predicted by the WWV index in June (third column) and the CTP index in June (fourth column). Columns 5–8 are the same as columns 1–4, but for La Niña events. Specifically, when a precursor is greater (less) than 40% of its standard deviation, then an El Niño (La Niña) is predicted. The year 1994 is neither WEP-type nor OCP-type El Niño.

		Predicted by				Predicted by	
El Niño year	TYPE	WWV_{JUN}	CTP_{JUN}	La Niña Year	TYPE	WWV_{JUN}	CTP_{JUN}
1982	WEP	✓	✓	1983	WEP	✓	✓
1986	WEP	✓	✓	1984	WEP	✓	✓
1987	OCP	×	✓	1988	WEP	✓	✓
1991	OCP	✓	✓	1995	WEP	✓	×
1994		×	×	1998	WEP	✓	✓
1997	WEP	✓	✓	1999	OCP	✓	✓
2002	OCP	✓	✓	2000	OCP	×	✓
2004	OCP	×	✓	2007	WEP	✓	✓
2006	WEP	✓	×	2008	OCP	×	✓
2009	WEP	✓	×	2010	WEP	✓	✓
2014	WEP	✓	✓	2011	OCP	×	✓
2015	OCP	✓	✓	2016	WEP	✓	✓
2018	WEP	✓	✓	2017	OCP	×	×

equatorial region, so this anomaly translates into about a 30% reduction of the annual mean equatorial undercurrent (~60 cm s^{-1}; Fig. 11b). It indicates that the anomalous current associated with ENSO is quite strong, so its contribution to the subsurface temperature tendency could be nontrivial.

Unlike the WEP type, where current anomalies show a reversal, the spatial patterns of zonal and meridional current anomalies are relatively stationary for the OCP type. For example, strong poleward (equatorward) meridional current anomalies are located west (east) of 140°W during FMA(0) (Fig. 10e). The meridional current anomalies persist from FMA(0) to the ENSO peak in NDJ(0). According to the recharge/discharge mechanism, the evolution of meridional convergence/divergence (recharge/discharge process) plays a primary role in modulating the equatorial thermocline anomalies. However, for the OCP type, the continuation of the meridional current anomalies indicates that other dynamical processes must play an active role in modulating the equatorial subsurface temperature anomalies.

5. Physical processes contributing to the two types of ENSO

The previous section suggests that both anomalies in the WE Pacific and OE region can modulate the CE thermocline. In this section, we discuss results from a more detailed heat budget analysis using GODAS data to clarify the relative contributions of advection terms to the thermocline temperature tendency for the WEP and OCP types.

As the first step, it is important to know whether GODAS analysis can reproduce the observed current structures. GODAS exhibits two shallow meridional overturning circulations straddling each side of the equator, where water in the subtropical mixed layer is subducted into the thermocline layer and then moves equatorward to feed the Equatorial Undercurrent (Fig. 11). At the equator, this water is upwelled into the mixed layer, then moved poleward by the Ekman transport. The equatorward flow across 8°S in the Southern Hemisphere (an important region to measure the strength of subtropical cells; e.g., McPhaden and Zhang 2002) is stronger than its northern counterpart. These features are part of the typical STCs in the Pacific Ocean documented from observational and model studies (McCreary and Lu 1994; Schott et al. 2004).

Within the STCs, there are two narrow meridional overturning cells confined within the deep tropics (0°–6°N/S), which are manifested by maximums in the meridional current around 4°S/4°N near 100 m (Fig. 11c). These two cells have been referred to as tropical cells (TCs; Lu et al. 1998), which are associated with the downwelling driven by the decrease in the poleward Ekman transport 4°–6° off the equator. Overall, the currents in GODAS are largely consistent with previous observational and modeling studies (Liu 1994; McCreary and Lu 1994; Johnson et al. 2001; Schott et al. 2004). This analysis gives us confidence that we can use GODAS to diagnose the physical processes modulating thermocline anomalies in the CE Pacific.

In the literature, the importance of the interaction between the off-equatorial and the equatorial anomalies via meridional currents is mostly discussed on decadal time scales, partially because of slow advective processes. STCs are considered a major pathway linking subtropical thermal signals to equatorial variations (Gu and Philander 1997). The meridional current speeds in the thermocline around 8°S/8°N, where the amplitude of the transport is used as a measure the strength of STC (McPhaden and Zhang 2002), is about 1 cm s^{-1} (Fig. 11c). Given this current speed, it would take years for the anomalies to advect from the subtropics to the equator. On the other hand, the equatorward maximum of the TCs is about 3 cm s^{-1}. It takes a water parcel about 1.5 months to travel 1° of latitude. If the off-equatorial subsurface anomalies are close to the equator, like around 3°–4°S/N, off-equatorial subsurface anomalies can be carried toward the equator within months, and then affect equatorial SST anomalies via vertical advection. This suggests that meridional advection by the mean

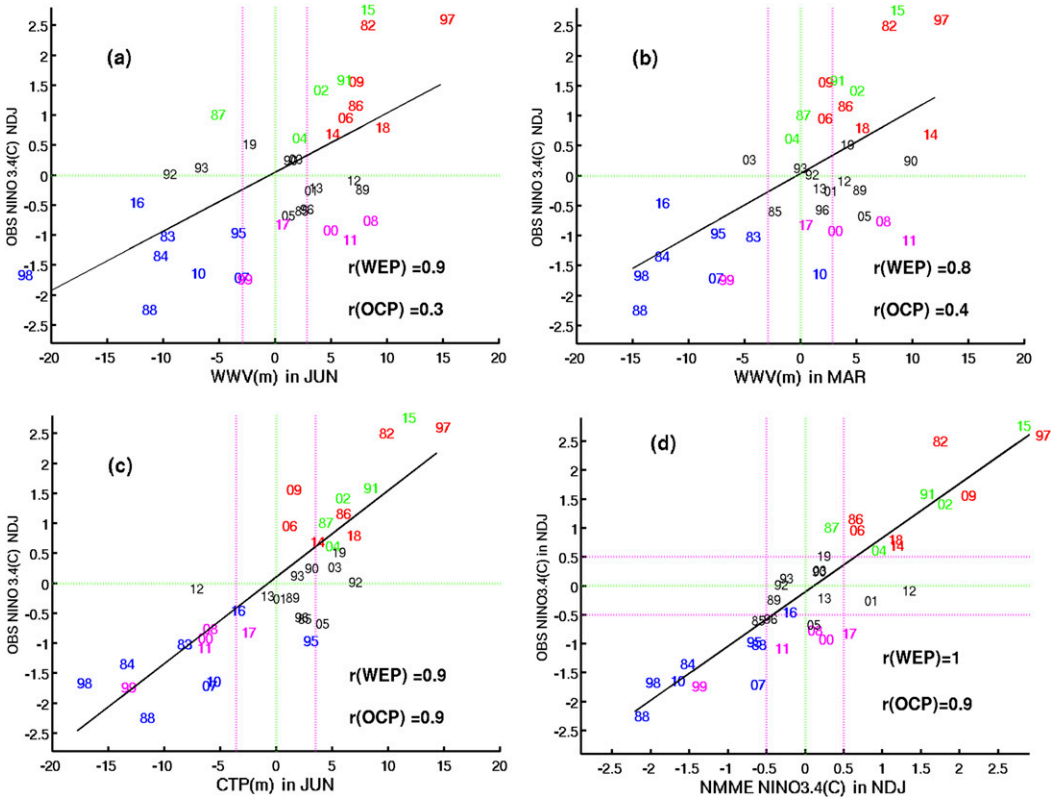

FIG. 7. Scatterplot of (a) WWV in June, (b) WWV in March, (c) CTP in June, and (d) NMME Niño-3.4 forecasts initialized at early July vs observed Niño-3.4 indices in NDJ during 1982–2019. In (a)–(c), purple dashed lines denote the threshold values of the two precursors. Here r(WEP) denotes the correlation coefficient for the WEP events and r(OCP) denotes the correlation coefficient for the OCP events. Correlation values greater than 0.5 are significant well above the 95% confidence level. Numerals denote the last two digits of the year. The red (blue), green (purple), and black characters represent WEP El Niño (La Niña), OCP El Niño (La Niña), and ENSO neutral years, respectively. Note that 1994 El Niño was not included in the plot because it is neither WEP El Niño nor OCP El Niño.

meridional current could be an important driver of equatorial thermocline variations on seasonal time scales.

In the tropical Pacific Ocean, the upper-ocean mixed and thermocline layers are relatively active. The deeper ocean, below the thermocline layer, is relatively stable. The upper ocean can be described by a 2.5-layer reduced gravity ocean model (Schopf and Cane 1983; McCreary and Yu 1992). The D20 variations are linearly proportional to the variations of subsurface temperature in the thermocline layer (i.e., a shallower D20 means cooler subsurface temperature in the thermocline). The processes that contribute to equatorial D20 variations are identical to the processes driving equatorial thermocline temperature variations.

The temperature equation in the second layer (thermocline layer) can be described as

$$\frac{\partial T_2}{\partial t} = -u_2\frac{\partial T_2}{\partial x} - v_2\frac{\partial T_2}{\partial y} + \text{residual},$$

where T_2, u_2, and v_2 represent the thermocline temperature, zonal current, and meridional current, respectively (McCreary and Yu 1992; Lee and Csanady 1999; Wen et al. 2010). In this study, T_2 is defined as the temperature average from the depth of 20°C to the depth of the mixed layer $\int_{h_{D20}}^{h_{mld}} TdZ/(h_{D20} - h_{mld})$. Similarly, u_2 is defined as $\int_{h_{D20}}^{h_{mld}} u_2 dZ/(h_{D20} - h_{mld})$, and v_2 is defined as $\int_{h_{D20}}^{h_{mld}} u_2 dZ/(h_{D20} - h_{mld})$. Note that the definitions of u_2 and v_2 are the same as in section 4. The residual includes the solar radiation fluxes penetrating through the mixed layer, the heat flux exchange between the mixed layer and the thermocline layer, the heat flux exchange between the thermocline and the deeper ocean, the vertical downwelling process, and the diffusion processes, which are not the focus of this study.

Here, we use the horizontal heat advection analysis to identify key drivers of the equatorial thermocline temperature. The advective fluxes across each side of the CE Pacific (green boxes) is noted by the arrows in Fig. 12. To avoid dependence on temperature scale (°C or K), we calculated the heat transport using a modified scheme following Lee et al. (2004):

$$\frac{\partial T_2}{\partial t} = -\frac{\partial U_2(T_2 - T_m)}{\partial x} - \frac{\partial V_2(T_2 - T_m)}{\partial y} + \text{residual},$$

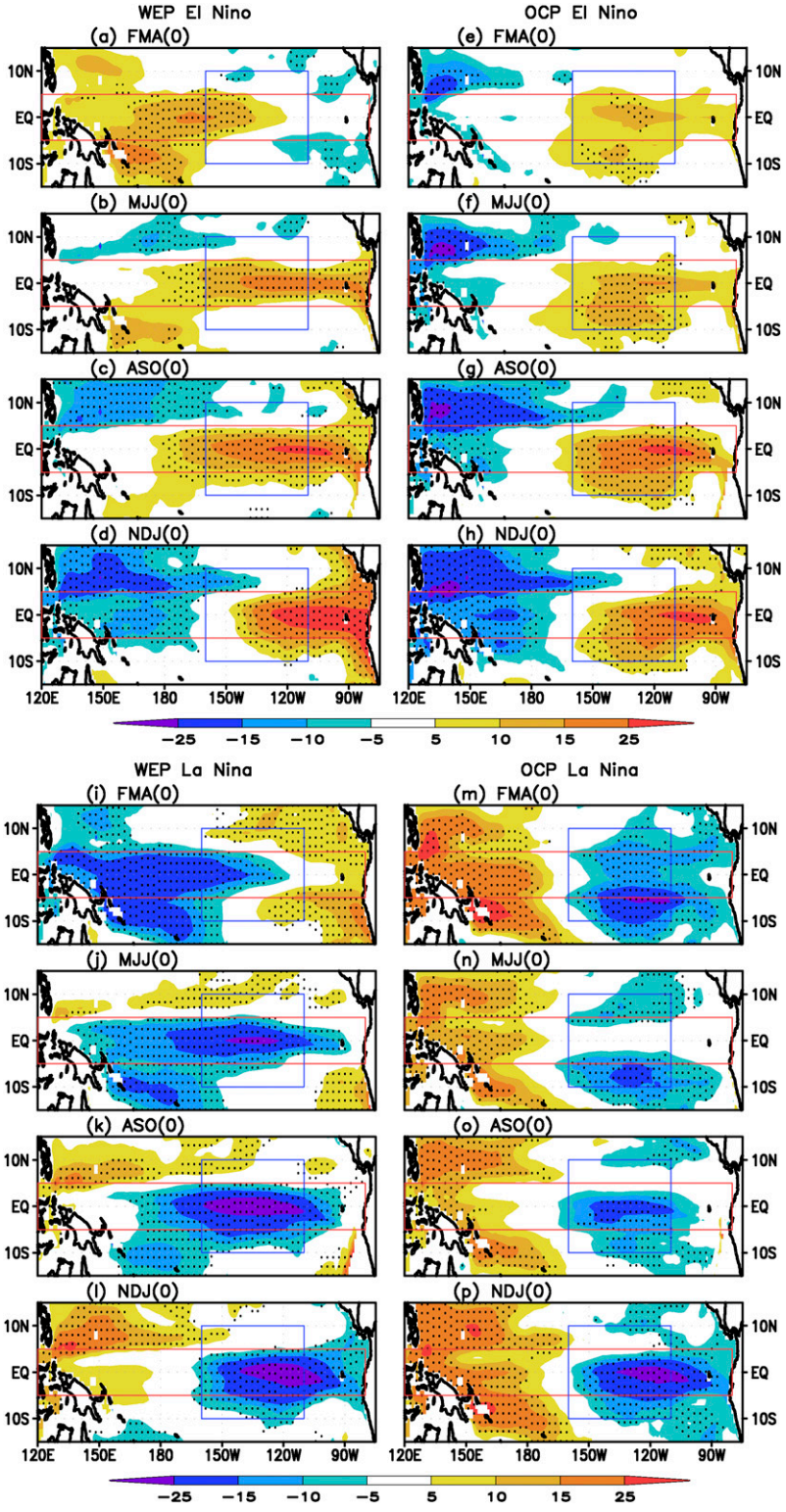

FIG. 8. El Niño composites of D20 anomalies (m) for the (a)–(d) WEP type and (e)–(h) OCP type, where (0) indicates the El Niño year. (i)–(p) As in (a)–(h), but for La Niña composites. Shading denotes the ensemble mean of six ocean reanalysis products; dotted areas are significant at the 90% statistical significance level using the Student's *t* test. Blue and red boxes display regions used to define WWV and CTP precursors, respectively.

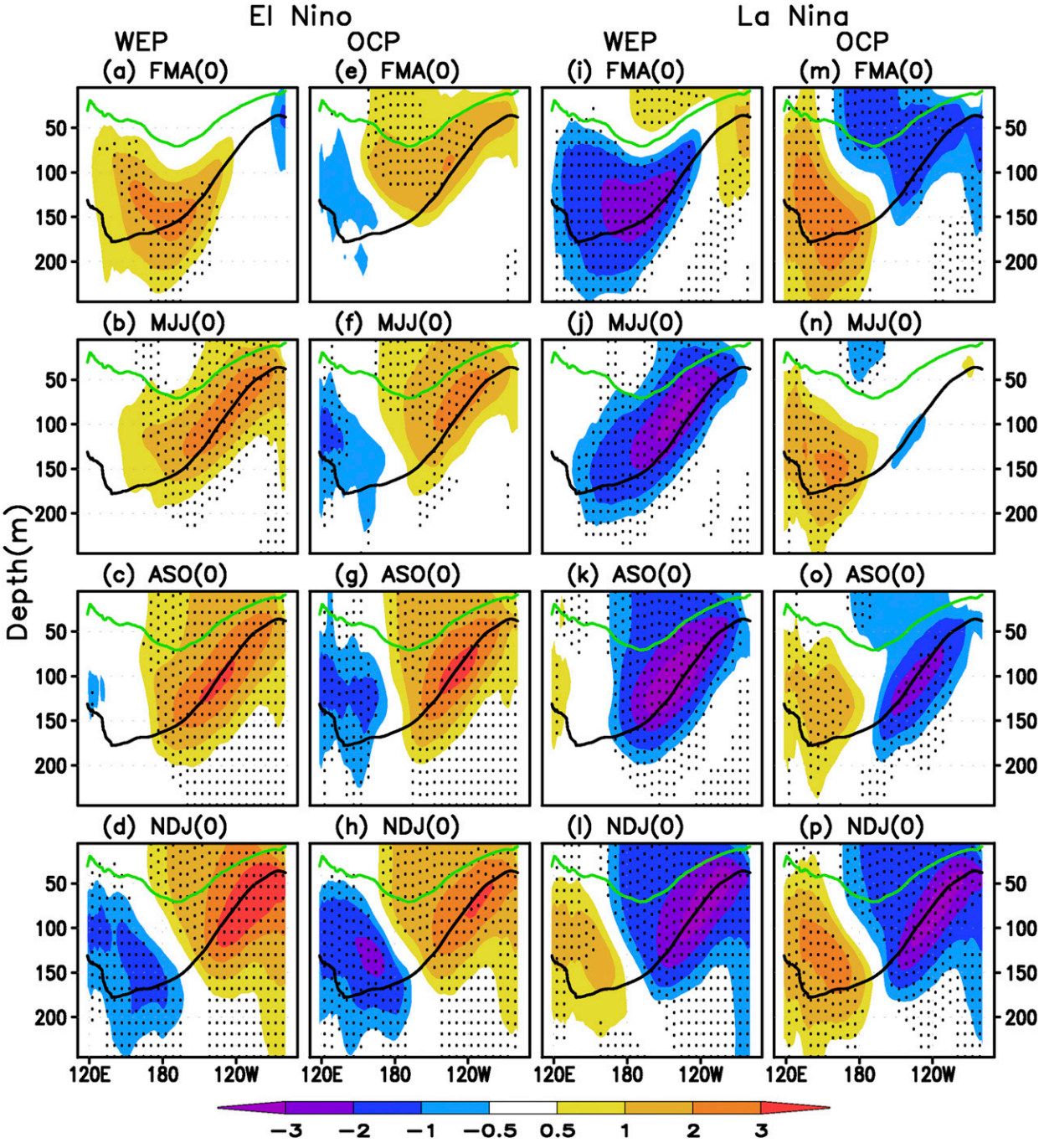

FIG. 9. Composites of upper ocean temperature anomalies (°C) along the equator (2°S–2°N) for (a)–(d) WEP-type and (e)–(h) OCP-type El Niño, where (0) indicates the El Niño year. Green and black lines in each panel are the climatology mean of mixed layer depth and D20 from GODAS. Shading denotes the ensemble mean of six ocean reanalysis products and dotted area are significant at the 90% statistical significance level using the Student's t test. (i)–(q) As in (a)–(h), but for the La Niña composites.

where T_m is the volume-averaged temperature in the domain of interest. By using the average temperature as a reference, this scheme does not depend on the definition of temperature scale and does not require zero net mass flux across each section (Lee et al. 2004; Kim et al. 2007; Zhang and McPhaden 2010). The first two terms on the right side represent the zonal and meridional heat advection, respectively. The residual represents other processes not included in the horizontal advection term.

The advection terms on interannual time scales can be decomposed as

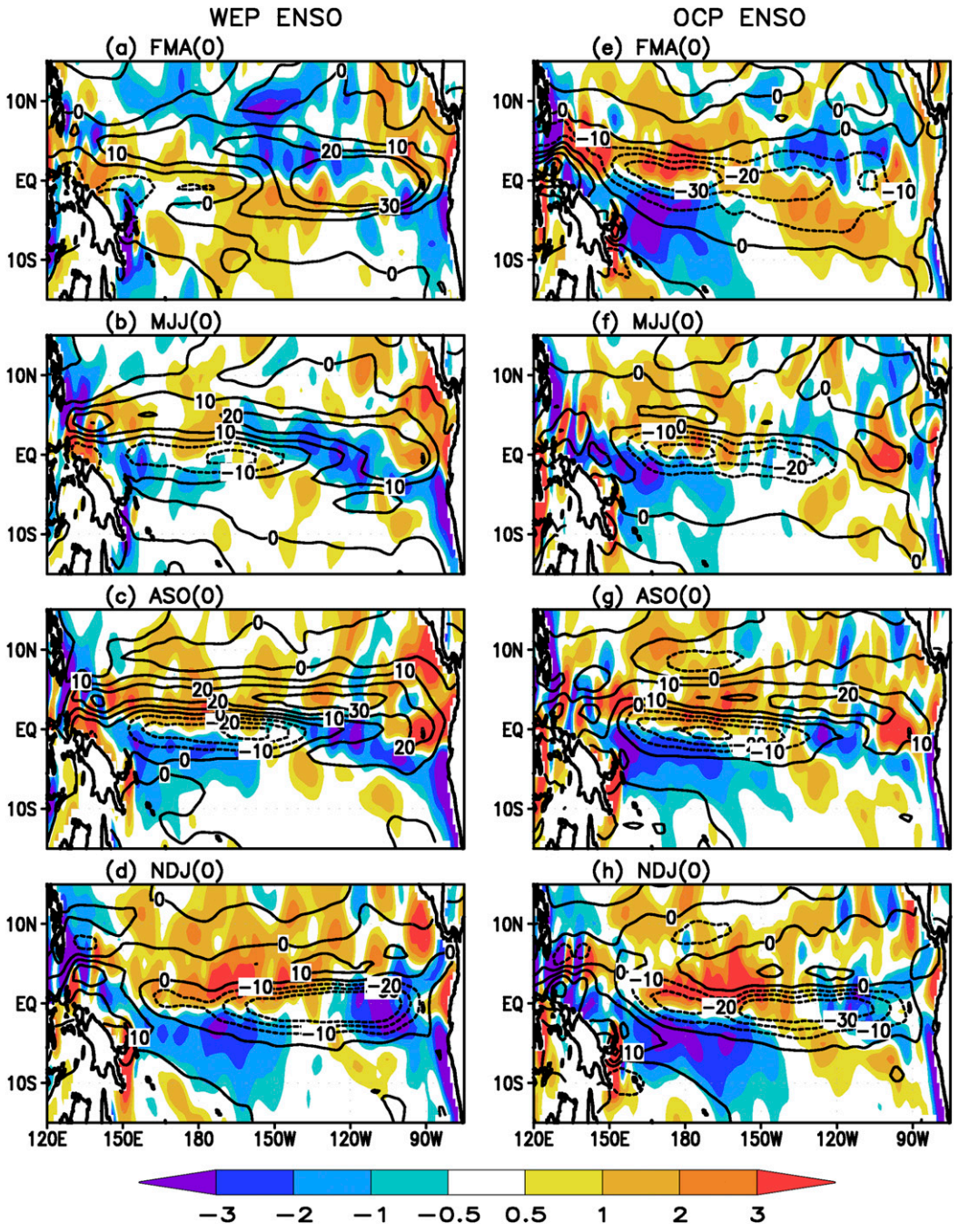

FIG. 10. ENSO composites (El Niño minus La Niña) of thermocline zonal (contours; positive for eastward) and meridional current anomalies (shaded; positive for northward) for the (left) WEP-type and (right) OCP-type ENSO; (0) indicates the ENSO year. Current unit is in cm s^{-1}.

$$U_2(T_2 - T_m) = U_2'(\overline{T_2 - T_m}) + \overline{U_2}(T_2 - T_m)' + U_2'(T_2 - T_m)',$$

$$V_2(T_2 - T_m) = V_2'(\overline{T_2 - T_m}) + \overline{V_2}(T_2 - T_m)' + V_2'(T_2 - T_m)',$$

where the overbar denotes monthly climatology cycles and primes denote departures from these cycles. Advection consists of three terms: the advection of mean temperature by anomalous flow, the advection of anomalous temperature by the mean flow, and the anomalous advection of anomalous temperature (nonlinear term).

For the WEP type (Figs. 13a,b), zonal advection plays an important role in modulating the temperature tendency ($\partial T_2/\partial t$) (black lines). The zonal advection of mean temperature by anomalous flow (blue lines) is in phase with $\partial T_2/\partial t$,

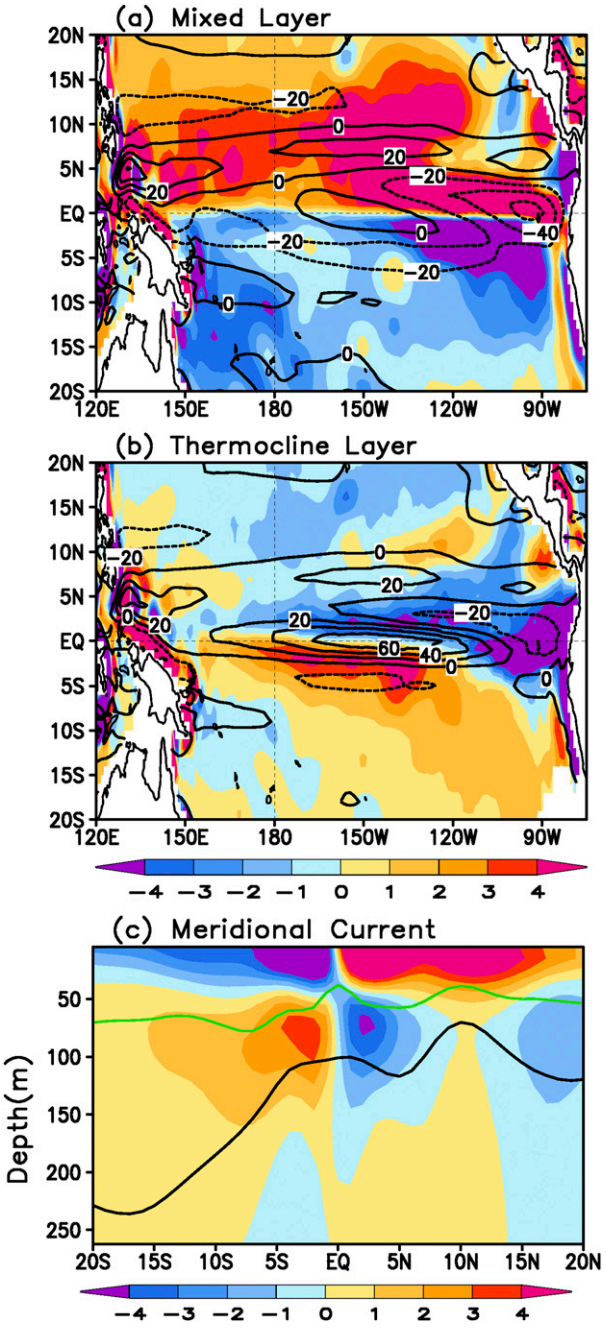

FIG. 11. Annual mean zonal (contours; positive value is eastward) and meridional currents (shaded; positive value is northward) in the (a) mixed layer, (b) thermocline layer, and (c) annual mean meridional currents averaged over 170°–110°W as a function of depth from GODAS. Current unit is cm s^{-1}. In (c), green and black lines indicate the climatological mean depth of the mixed layer and the depth of 20°C in GODAS, respectively.

suggesting its important role in the onset and decay of ENSO. The contribution of zonal advection of anomalous temperature by the mean flow (green lines) is strongest from early summer to the mature phase of ENSO. It suggests that this term is important during the onset and development of ENSO. After the peak ENSO, the zonal advection of anomalous temperature appears to contribute to the El Niño transition to La Niña in the following spring, MAM(1)–MJJ(1), while it continues to be one phase through MJJ(1) for the WEP La Niña composite. The meridional advection is dominated by the anomalous temperature by the mean flow (red lines). The meridional advection tends to enhance and maintain the thermocline temperature in the CE region. The nonlinear term (dashed purple lines) tends to damp $\partial T_2/\partial t$ during the onset and development of ENSO. The residual term (orange dashed lines) is in the same phase with the temperature tendency during January–March [JFM(0)] to MJJ(0) and then it switches sign. This suggests the residual term also contributes to the onset and the development of WEP ENSO during JFM(0) to MJJ(0), and then contributes to the decay and ENSO transition.

The relative contribution of advection terms in the OCP type is quite different with those for the WEP type. During the development of OCP-type El Niño (Fig. 13c), heat advection carried by the mean meridional current (red lines) and zonal current (green lines) are the two largest terms contributing to the $\partial T_2/\partial t$, while the contribution of the mean temperature carried by the anomalous flow is negligible. It is noteworthy that the event-to-event spread of zonal advection (green bars) is larger than the mean (i.e., the signal; green line), suggesting the large uncertainty among the five OCP El Niño events. In contrast, the mean signal of meridional advection is consistently greater than the spread since MAM (0) season although its amplitude is slightly weaker than the zonal advection during MJJ(0) through July–September [JAS(0)]. This indicates that the contribution of the zonal advection might depend on individual events, while the contribution of anomalous meridional advection ($\overline{V}T'$) is a robust feature among the OCP El Niño. It is noteworthy that the residual term follows closely with the temperature tendency since JAS(0), suggesting its important role in the decay and transition of OCP El Niño.

During the onset and development of OCP type La Niña [JFM(0)–JAS(0)] (Fig. 13d), the advection of anomalous temperature carried by the mean meridional currents (red line) clearly plays the primary role in modulating $\partial T_2/\partial t$. This is because all other advection terms remain positive and do not contribute to negative $\partial T_2/\partial t$. In addition, the mean signal of meridional advection is consistently greater than the spread during the course of La Niña evolution. It suggests the contribution of meridional advection is a common feature to all OCP-driven La Niña events.

We note that the meridional heat advection by the mean current for the OCP El Niño composites during JFM(0)–MJJ(0) is weaker than that for the OCP La Niña, and the temperature tendency is relatively small during the El Niño onset. These features might be associated with the asymmetric atmospheric and oceanic response between El Niño and La Niña. Previous studies suggested that tropical wind has a stronger response to a positive SST anomaly than to a negative SSTA (Okumura et al. 2011; Choi et al. 2013) and oceanic response is more sensitive to the surface winds during El Niño

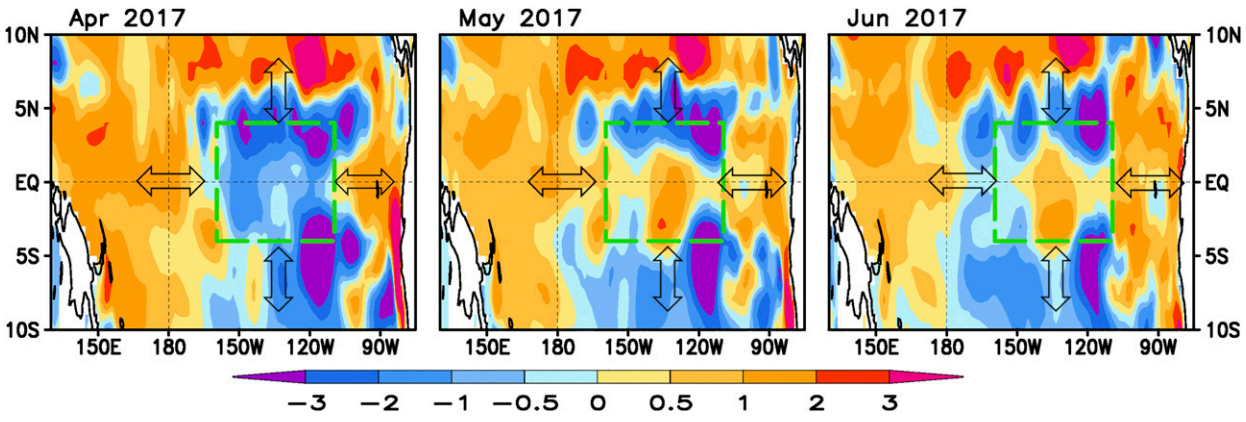

FIG. 12. Thermocline temperature anomalies (°C) averaged in the thermocline layer during April–June 2017. Thermocline temperature is defined as the average of temperature from depth of 20°C to the depth of the mixed layer from GODAS. The green rectangles (160°–110°W, 5°S–5°N) indicate the domain for the integrative thermocline layer heat budget analysis and arrows illustrate the horizontal heat advection schemes.

than during La Niña because of shallower thermocline depth in the western tropical Pacific, which efficiently traps the atmospheric momentum in the shallow upper ocean (An and Kim 2017). Weak subsurface warming together with the stochastic westerly wind forcings could easily induce a rapid SST warming and air–sea coupling in the deep tropical Pacific. Surface processes (e.g., zonal advection feedback, surface heat flux, etc.) can also play an important role to boost the El Niño development.

The heat budget analysis suggests that the OE anomalous thermocline temperature carried by the mean meridional current plays an important role in the onset of OCP type and multiyear La Niña events. To our knowledge, this contribution is rarely discussed in the literature. The meridional advection associated with the mean current can work either constructively or destructively with other processes. Its impact can sometimes outweigh the influence of zonal advection and take on the dominant role, thereby becoming an important feature for the OCP type. For example, in May 2017, there was a rapid eastward propagation from the WE Pacific to the eastern equatorial Pacific owing to downwelling Kelvin waves (Fig. 12). The positive subsurface temperature anomalies were confined within a narrow equatorial band (3°S–3°N), while negative temperature anomalies persisted in the OE regions. The negative temperature anomalies advected by the mean meridional current eventually dominated the warming tendency and resulted in a La Niña. It is noteworthy that all of the multiple ocean reanalyses display similar spatial patterns and evolution with the ensemble mean during 2017. However, the location and intensity of D20 anomaly centers vary slightly among the individual reanalysis products, giving rise to the large uncertainty of CTP index during 2017 (Fig. 1b). This suggests that in addition to monitoring ENSO precursor indices, it is important to monitor the spatial distribution and evolution of the D20 anomaly for ENSO monitoring and prediction. Such information can provide insights to understand the complex interaction between the off-equatorial advection and other processes, as well as to understand the uncertainty in precursors.

6. Summary and discussion

ENSO prediction skills of dynamical models utilizing subsurface conditions saw a degradation in the twenty-first century. This reduced skill coincided with a decline in the utility of WWV as a useful precursor for ENSO, leading to the question of whether other oceanic processes may have become more important. Using a set of ocean reanalysis products, we reassessed prediction skills of two oceanic precursors, WWV and CTP, during the so-called spring barrier period (i.e., April–June) for observed ENSO events after 1980. The dynamical processes linking different oceanic preconditions with ENSO onsets were investigated via ENSO composites and heat budget analysis (also referred to as anomalous horizontal heat advection diagnostic). We identified two ENSO categories based on spatial and temporal connections between the central equatorial D20 variations and surrounding regions. Based on the precursor mechanisms, we also found that the importance of the two precursors to ENSO onset is tightly connected with the two newly defined categories of ENSO. Our major findings are as follows:

1) The western equatorial Pacific driven ENSO is characterized by eastward propagating D20 anomalies from the western to eastern Pacific during the onset and development phase of ENSO. This type of ENSO is mostly accompanied by an east–northwest seesaw pattern during the ENSO development and mature phases that leads to ENSO phase transition. Zonal heat advection plays a crucial role in modulating the CE subsurface tendency.
2) The off-equatorial central Pacific (OCP)-driven ENSO is characterized by a stationary east–west dipole pattern in the D20 anomaly during the entire ENSO evolution cycle. Subsurface temperature anomalies carried by mean

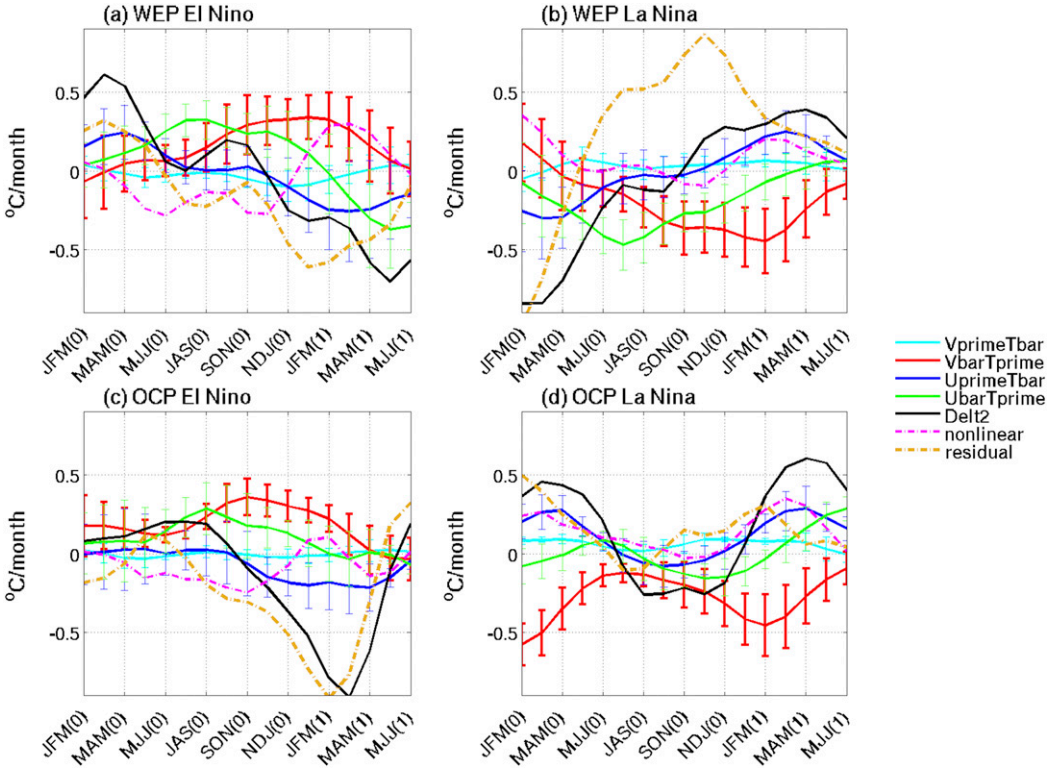

FIG. 13. Composite of thermocline temperature tendency (black line) and advection terms in the thermocline layer average in the box (160°–110°W, 5°S–5°N) for the (a) WEP El Niño events, (b) WEP La Niña events, (c) OCP El Niño events, and (d) OCP La Niña events. Cyan and red lines indicate the meridional advection by the mean temperature carried by anomalous current and by the temperature anomaly carried by the mean current, respectively. Blue and green lines indicate the zonal advection by the mean temperature carried by anomalous current and by the temperature anomaly carried by the mean current, respectively. Purple dash-dotted lines represent the nonlinear advection terms. Orange dashed lines represent the residual term. Error bars imposed on each advection term represent one standard deviation of the composite ENSO events. The 3-month running mean apply to all the anomalies.

meridional currents play a primary role during the central equatorial subsurface warming (cooling) preceding El Niño (La Niña) onset. Zonal advection is most important for the phase transition of central equatorial thermocline variations after the development of the OCP ENSO events.

3) WWV accurately predicts all the WEP-driven ENSO events with 6–9-month lead (15 out of 15 cases), while WWV was a poor precursor for most OCP-driven ENSO events (6 out of 10 cases failed). In contrast, CTP not only is a particularly good precursor for OCP-type onsets (9 out of 10 cases), but also it has a robust lead correlation with WEP-type events. The importance of CTP as an ENSO precursor is more evident after 1999. The difference in the two precursors highlights the importance of off-equatorial subsurface preconditions on the ENSO onsets.

We demonstrated that the variation of CE subsurface temperature is dynamically linked with multiple horizontal advection mechanisms. An important finding of this study is that the subsurface branches of tropical cells play a vital role in linking the off-equatorial subsurface anomalies with the CE subsurface fluctuations on seasonal time scales. The efficacy of this meridional advection also depends on whether OE subsurface anomalies are close to the equator (around 4°S/N). These two factors together allow the OE subsurface anomalies to have a substantial influence on the equatorial subsurface variations within several months and hence can affect equatorial SST via vertical advection on seasonal time scales.

We also demonstrated that the western Pacific heat content variations can significantly affect the CE subsurface temperature variability either by the temperature anomalies carried by the equatorial undercurrent or by zonal heat advection by anomalous zonal currents. Our results support recent arguments that zonal transport is an important factor contributing to equatorial heat content variability (i.e., Ballester et al. 2016; Lu et al. 2017). It is noteworthy that our results suggest a minor contribution of meridional advection by anomalous currents on the CE subsurface temperature, and hence, seem to contradict the recharge/discharge paradigm. Indeed, the strong ENSO-related meridional current divergence/convergence

near the western-central equatorial regions could have an impact on the central equatorial subsurface temperature variability via adjusting the zonal transport along the Equatorial Undercurrent (Lu et al. 2017).

Our analysis suggests that the multiple oceanic processes can either act in concert to create a strong subsurface tendency in the central equatorial region or cancel each other out, and hence can contribute differently to prediction skill of individual ENSO events. If off-equatorial subsurface anomalies act destructively with the influence of western Pacific subsurface anomalies during the boreal spring season, preconditions in the western Pacific become less important to ENSO onset. This hypothesis is consistent with the poor long-lead predictive relationship between WWV and OCP-type ENSO and the strong predictive relationship for WEP-type ENSO. The constructive/destructive interference also offers an explanation for the decreased predictive utility of WWV for ENSO after the late 1990s, because whereas more than 70% of ENSO events before the late 1990s were WEP-type ENSO, fewer than 50% of ENSO events after were WEP type. A similar explanation can also apply to the poor predictive value of WWV for multiyear La Niña events, as 5 out of 6 were OCP-type ENSO.

ENSO prediction skills of dynamical models also declined in recent decades, and most models had low skill in predicting multiyear La Niña events (Timmermann et al. 2018). This gives rise to the question of whether ENSO predictability of the current generation of dynamical models also depends on ENSO types. To explore this, we compared the NMME forecast from 1 July initial conditions for the observed Niño-3.4 in NDJ during 1982–2019 (Fig. 7d). Similar to WWV precursor, skills of these state-of-the-art models depend on the specific type of ENSO. For example, NMME accurately predict ENSO conditions with a 6-month lead for all WEP-based ENSO events, while NMME failed to predict 50% of OCP-based ENSO events (1987 El Niño and the 2000, 2008, 2011, and 2017 La Niña events). A common feature of these events was that OE thermocline anomalies were opposite to the WE thermocline anomalies during early spring season, leading to a negative interference between opposite signals of OCPI and WEPI indices shown in Fig. 6. All the NMME models use ocean reanalysis as initial conditions, and off-equatorial anomalies, in principle, are present in the analysis. The interaction between OE and WE temperature anomalies presents a challenge for model predictions because it requires the models not only to represent both dynamics, but also to have the ability to capture the relative strength of each process. In the future, the relative roles of the OCP and WEP mechanisms should be examined to possibly explain the reduction of skill in dynamical models in recent decades. Further, the relative roles of the OCP and WEP mechanisms should also be examined to possibly explain the reduction of skill in dynamical models in recent decades—in particular, to determine whether initialization errors (i.e., biases in the representation of subsurface anomalies in off-equatorial thermocline regions) and/or errors in ocean dynamics explain why NMME models fail to predict some OCP-driven ENSO events.

Our analysis demonstrated that WWV and CTP precursors and D20 indices representing the D20 variation in the western-equatorial Pacific (WEPI), off-equatorial Pacific (OCPI), and central equatorial Pacific (CEPI) are very useful for ENSO monitoring and predictions. However, the location and the timing of the development of central equatorial thermocline variation vary with individual events. The indices defined with fixed box sometimes are not able to capture these details. Furthermore, the evolution of central equatorial thermocline variation is not a simple linear combination of the WE and OE preconditions. Instead, it involves complex multiple processes (i.e., oceanic Kelvin wave activities, atmospheric response, etc.), often in a nonlinear manner. It is a big challenge to make long lead prediction during the late winter–spring season when thermocline anomalies in the western Pacific region and central off-equatorial region are in opposite phases. In addition to monitoring these indices, it is thus also important to monitor the spatial distribution of D20 and its evolution. We showed that the evolutions of subsurface conditions related to the OCP and WEP ENSO have distinct features. For the real-time ENSO forecasting, when opposite D20 anomalies are present in the WE and OE regions during the spring season, it is important to check whether the D20 evolution resembles those OCP-driven ENSO composites: for example, examining whether off-equatorial signals are close to the equator, and whether the D20 anomalies weaken from the western Pacific to the central equatorial region. Such information will help forecasters to determine whether the off-equatorial signals play an important role in modulating central equatorial thermocline tendency, and to decide whether they can trust WWV and dynamical model forecasts when they have opposite projections to the CTP forecast.

It is noteworthy that we delineated ENSO events based on relative importance of precursor mechanisms in this study. It does not necessary imply that equatorial wave associated preconditions are not important for OCP-driven ENSO events. For example, for the 2002 and 2015 OCP El Niño, the equatorial wave-related processes still play an important role in triggering El Niño onsets. These processes work in concert with the off-equatorial precursors, modulating El Niño evolutions. Furthermore, our dynamically driven classification is different from the earlier classification (eastern Pacific vs central Pacific El Niño) that is based on the location of the maximum SST warming (e.g., Ashok et al. 2007; Kug et al. 2009; Yu et al. 2010). The SST pattern classification usually only refers to the warm events because cold events tend to peak farther west than the warm events and thus have much less difference in their spatial patterns. Interestingly, all of the OCP El Niño events (1987, 1991, 2002, 2004, and 2015) are also classified as central Pacific El Niño in the literature (e.g., Yu and Kim 2010; Paek et al. 2017). Our studies suggest that the impact of meridional heat advection in the subsurface offers a new perspective to understand the development of central Pacific El Niño.

Except for its spatial structure, ENSO is a complex phenomenon with a range of different amplitudes and temporal evolutions (Capotondi et al. 2015). In particular, some ENSO events are preceded by the same El Niño (La Niña) phase to become multiyear ENSO events. The frequency of multiyear La Niña events is higher than that of El Niño events in nature

(Okumura and Deser 2010). Recent studies have suggested that multiyear La Niña evolutions have a close relationship with midlatitude atmospheric variability via the Pacific meridional mode or seasonal footprinting mechanisms (Yu and Fang 2018; Park et al. 2020; Fang and Yu 2020). DiNezio et al. (2017a,b) suggested that 2-yr La Niñas may be predictable 18–24 months in advance when initialized with a strong thermocline discharge or a strong El Niño condition. Wu et al. (2019) analyzed the observation data and a long model simulation. They suggested that a strong El Niño preceding a La Niña not only induces a strong discharge, but also adjusts the SST response in the tropical Atlantic, which in turn induces easterly wind anomalies over the western equatorial Pacific, thus favoring development of a subsequent La Niña. The duration of El Niño events, on the other hand, depends on the timing of their onset. Their simulations also showed that ENSO tend to persist to a second year when the sign of thermocline depth anomalies remains the same in the central-eastern equatorial Pacific through the boreal spring following the first peak. Our analysis demonstrated that 7 out of 10 OCP ENSO events since 1982 (1987 and 2015 El Niño and 1999, 2000, 2008, 2011, and 2017 La Niña) have been preceded by the same phase of ENSO. Similar to Wu et al. (2019), the thermocline anomalies in the CE restrengthened during the late spring/summer for these events. As shown in Fig. 1b, these second- or third-year ENSO events are accompanied by persistent cold conditions during 1998–2001, 2007–09, 2010–13, and 2016–17 and warm conditions during 1986–87 and 2014–15 in the off-equatorial thermocline region. These persistent conditions occurred prior to the peak of the first-year ENSO. For the remaining OCP ENSO events (1991, 2002, and 2004), off-equatorial anomalies also coincide with the persistent warm conditions during 1990–94 and 2002–05. Our analysis suggested that contribution of persistent cold (warm) off-equatorial thermocline variations, via meridional advection, offer an alternative explanation for consecutive La Niña (El Niño) events. The low frequency of OE thermocline variations could, therefore, be important source for prediction of multiyear ENSO.

The frequency of OCP-driven ENSO events has increased fourfold since the start of the twenty-first century. Why are these changes occurring? One possibility is the decadal shift of climatological mean state in the tropical Pacific during the late 1990s. Wen et al. (2014) found that the strength of the subtropical cells' interior mass transport in both hemispheres increased rapidly around the late 1990s, which might be associated with enhanced easterly trade winds over the west-central tropical Pacific and deeper (shallower) D20 in the western (eastern) Pacific after the late 1990s (McPhaden et al. 2011; Xiang et al. 2013). The increased meridional current in the thermocline might help to explain the increased influence of OE thermocline variations on the ENSO onsets after the late 1990s. Another possibility is the decadal change in the WWV variability in the pre- and post-2000 periods. Neske and McGregor (2018) demonstrated that the adjusted wind response (long-lead time predictable part) contribution to WWV variability is reduced substantially, whereas the instantaneous response dominates WWV variability post-2000. Neske et al. (2021) recently linked the decadal change in WWV variability with the surface wind curl pattern changes in the tropical Pacific. The decline of adjusted wind response contribution to WWV provides opportunity for other processes; for example, meridional heat advection has played a more important role in ESNO onset since the twenty-first century. Further studies using a longer observational record or model simulations are needed to clarify the causes of the change in frequency.

It is recognized that ENSO events differ in amplitude, temporal evolution, and spatial pattern (Capotondi et al. 2015). Previous studies articulated the importance of timing and strength of high-frequency atmospheric forcing on ENSO diversity (Chen et al. 2015). Our results are in concert with previous studies because thermocline variations in the western Pacific, which integrate oceanic Kelvin wave activities triggered by atmospheric forcing, play an important role in modulating ENSO evolution via zonal advection in the thermocline. Our results also suggest the low-frequency contribution of OE thermocline anomalies could play an important role in affecting ENSO characteristics. The constructive/destructive interference among the multiple processes on driving the CE subsurface temperature variability offers an alternate perspective to explain ENSO diversity. Our results support the notion that ENSO events can be better described as a broad continuum (e.g., Giese and Ray 2011; Capotondi et al. 2015).

Our results suggested that OCP-driven ENSO tends to be the central Pacific type of El Niño or multiyear ENSO. The present study did not discuss the characteristic features of the OCP-driven and the WEP-driven related atmospheric anomalies. Previous studies have suggested that extratropical variability can induce surface wind anomalies, which favor the central Pacific–type El Niño development (e.g., Yu et al. 2010; You and Furtado 2017; Luo et al. 2017) or multiyear La Niña events (e.g., Yu and Fang 2018; Park et al. 2020; Fang and Yu 2020). It is important to examine whether the extratropical variability-related wind anomalies also favor of triggering OCP-type ENSO. Further investigation is needed to explore physical processes inducing the off-equatorial anomalies, such as through local air–sea coupling, extratropical teleconnections, or interbasin teleconnections with the Indian Ocean and/or Atlantic Ocean.

The current operational ocean analysis products only span from 1979. Analysis with a longer observation period is also needed to validate our studies. Finally, our analysis of dynamical processes associated with thermocline variations is based on a single reanalysis product. Given the large uncertainties in the quantification of subsurface variability in the ocean reanalysis products, studies with other ocean and observation analyses are desirable for examining the robustness of our findings.

Acknowledgments. We thank Dr. Yuko M Okumura and three anonymous reviewers for their critical and constructive comments, which significantly improved the manuscript.

REFERENCES

Alexander, M. A., D. J. Vimont, P. Chang, and J. D. Scott, 2010: The impact of extratropical atmospheric variability on ENSO: Testing the seasonal footprinting mechanism using coupled model experiments. *J. Climate*, **23**, 2885–2901, https://doi.org/10.1175/2010JCLI3205.1.

An, S.-I., and J.-W. Kim, 2017: Role of nonlinear ocean dynamic response to wind on the asymmetrical transition of El Niño and La Niña. *Geophys. Res. Lett.*, **44**, 393–400, https://doi.org/10.1002/2016GL071971.

Ashok, K., S. K. Behera, S. A. Rao, H. Weng, and T. Yamagata, 2007: El Niño Modoki and its possible teleconnection. *J. Geophys. Res.*, **112**, C11007, https://doi.org/10.1029/2006JC003798.

Ballester, J., D. Petrova, S. Bordoni, B. Cash, M. García-Díez, and X. Rodó, 2016: Sensitivity of El Niño intensity and timing to preceding subsurface heat magnitude. *Sci. Rep.*, **6**, 36344, https://doi.org/10.1038/srep36344.

Barnston, A. G., M. K. Tippett, M. L. L'Heureux, S. Li, and D. G. DeWitt, 2012: Skill of real-time seasonal ENSO model predictions during 2002–11: Is our capability increasing? *Bull. Amer. Meteor. Soc.*, **93**, 631–651, https://doi.org/10.1175/BAMS-D-11-00111.1.

Battisti, D. S., and A. C. Hirst, 1989: Interannual variability in a tropical atmosphere–ocean model: Influence of the basic state, ocean geometry, and nonlinearity. *J. Atmos. Sci.*, **46**, 1687–1712, https://doi.org/10.1175/1520-0469(1989)046<1687:IVIATA>2.0.CO;2.

Becker, E., B. P. Kirtman, and K. Pegion, 2020: Evolution of the North American multi-model ensemble. *Geophys. Res. Lett.*, **47**, e2020GL087408, https://doi.org/10.1029/2020GL087408.

Behringer, D. W., and Y. Xue, 2004: Evaluation of the Global Ocean Data Assimilation System at NCEP: The Pacific Ocean. *Preprints, Eighth Symp. on Integrated Observing and Assimilation Systems for Atmosphere, Oceans, and Land Surface*, Seattle, WA, Amer. Meteor. Soc., 2.3, http://ams.confex.com/ams/84Annual/techprogram/paper_70720.htm.

Bonjean, F., and G. S. E. Lagerloef, 2002: Diagnostic model and analysis of the surface currents in the tropical Pacific Ocean. *J. Phys. Oceanogr.*, **32**, 2938–2954, https://doi.org/10.1175/1520-0485(2002)032<2938:DMAAOT>2.0.CO;2.

Capotondi, A., and Coauthors, 2015: Understanding ENSO diversity. *Bull. Amer. Meteor. Soc.*, **96**, 921–938, https://doi.org/10.1175/BAMS-D-13-00117.1.

Chang, P., L. Zhang, R. Saravanan, D. J. Vimont, J. C. H. Chiang, L. Ji, H. Seidel, and M. K. Tippett, 2007: Pacific meridional mode and El Niño–Southern Oscillation. *Geophys. Res. Lett.*, **34**, L16608, https://doi.org/10.1029/2007GL030302.

Chen, D., and Coauthors, 2015: Strong influence of westerly wind bursts on El Niño diversity. *Nat. Geosci.*, **8**, 339–345, https://doi.org/10.1038/ngeo2399.

Chiodi, A. M., and D. E. Harrison, 2015: Equatorial Pacific easterly wind surges and the onset of La Niña events. *J. Climate*, **28**, 776–792, https://doi.org/10.1175/JCLI-D-14-00227.1.

Choi, K.-Y., G. A. Vecchi, and A. T. Wittenberg, 2013: ENSO transition, duration, and amplitude asymmetries: Role of the nonlinear wind stress coupling in a conceptual model. *J. Climate*, **26**, 9462–9476, https://doi.org/10.1175/JCLI-D-13-00045.1.

Dee, D. P., and Coauthors, 2011: The ERA-Interim reanalysis: Configuration and performance of the data assimilation system. *Quart. J. Roy. Meteor. Soc.*, **137**, 553–597, https://doi.org/10.1002/qj.828.

DelSole, T., and M. K. Tippett, 2016: Forecast comparison based on random walks. *Mon. Wea. Rev.*, **144**, 615–626, https://doi.org/10.1175/MWR-D-15-0218.1.

Diebold, F. X., and R. S. Mariano, 1995: Comparing predictive accuracy. *J. Bus. Econ. Stat.*, **13**, 253–263.

DiNezio, P. N., C. Deser, Y. M. Okumura, and A. Karspeck, 2017a: Predictability of 2-year La Niña events in a coupled general circulation model. *Climate Dyn.*, **49**, 4237–4261, https://doi.org/10.1007/s00382-017-3575-3.

——, and Coauthors, 2017b: A 2 year forecast for a 60–80% chance of La Niña in 2017–2018. *Geophys. Res. Lett.*, **44**, 11 624–11 635, https://doi.org/10.1002/2017GL074904.

Fang, S. W. and J. Y. Yu, 2020: Contrasting transition complexity between El Niño and La Niña: Observations and CMIP5/6 models. *Geophys. Res. Lett.*, **47**, e2020GL088926, https://doi.org/10.1029/2020GL088926.

Farneti, R., S. Dwivedi, F. Kucharski, F. Molteni, and S. M. Griffies, 2014: On Pacific subtropical cell variability over the second half of the twentieth century. *J. Climate*, **27**, 7102–7112, https://doi.org/10.1175/JCLI-D-13-00707.1.

Fedorov, A. V., 2002: The response of the coupled tropical ocean–atmosphere to westerly wind bursts. *Quart. J. Roy. Meteor. Soc.*, **128** (579), 1–23, https://doi.org/10.1002/qj.200212857901.

——, S. Hu, M. Lengaigne, and E. Guilyardi, 2015: The impact of westerly wind bursts and ocean initial state on the development, and diversity of El Niño events. *Climate Dyn.*, **44**, 1381–1401, https://doi.org/10.1007/s00382-014-2126-4.

Giese, B. S., and S. Ray, 2011: El Niño variability in simple ocean data assimilation (SODA), 1871–2008. *J. Geophys. Res.*, **116**, C02024, https://doi.org/10.1029/2010JC006695.

Gu, D., and S. G. Philander, 1997: Interdecadal climate fluctuations that depend on exchanges between the tropics and extratropics. *Science*, **275**, 805–807, https://doi.org/10.1126/science.275.5301.805.

Hong, L.-C., LinHo, and F.-F. Jin, 2014: A Southern Hemisphere booster of super El Niño. *Geophys. Res. Lett.*, **41**, 2142–2149, https://doi.org/10.1002/2014GL059370.

Horii, T., I. Ueki, and K. Hanawa, 2012: Breakdown of ENSO predictors in the 2000s: Decadal changes of recharge/discharge–SST phase relation and atmospheric intraseasonal forcing. *Geophys. Res. Lett.*, **39**, L10707, https://doi.org/10.1029/2012GL051740.

Hu, S., and A. V. Fedorov, 2016: Exceptionally strong easterly wind burst stalling El Niño of 2014. *Proc. Natl. Acad. Sci. USA*, **113**, 2005–2010, https://doi.org/10.1073/pnas.1514182113.

Hu, Z.-Z., A. Kumar, B. Huang, J. Zhu, M. L'Heureux, M. J. McPhaden, and J.-Y. Yu, 2020: The interdecadal shift of ENSO properties in 1999/2000: A review. *J. Climate*, **33**, 4441–4462, https://doi.org/10.1175/JCLI-D-19-0316.1.

Izumo, T., M. Lengaigne, J. Vialard, I. Suresh, and Y. Planton, 2019: On the physical interpretation of the lead relation between warm water volume and the El Niño Southern Oscillation. *Climate Dyn.*, **52**, 2923–2942, https://doi.org/10.1007/s00382-018-4313-1.

Jin, E. K., and Coauthors, 2008: Current status of ENSO prediction skill in coupled ocean–atmosphere models. *Climate Dyn.*, **31**, 647–664, https://doi.org/10.1007/s00382-008-0397-3.

Jin, F.-F., 1997: An equatorial ocean recharge paradigm for ENSO. Part I: Conceptual model. *J. Atmos. Sci.*, **54**, 811–829, https://doi.org/10.1175/1520-0469(1997)054<0811:AEORPF>2.0.CO;2.

Johnson, G. C., M. J. McPhaden, and E. Firing, 2001: Equatorial Pacific Ocean horizontal velocity, divergence, and upwelling. *J. Phys. Oceanogr.*, **31**, 839–849, https://doi.org/10.1175/1520-0485(2001)031<0839:EPOHVD>2.0.CO;2.

Kanamitsu, M., W. Ebisuzaki, J. Woollen, S. K. Yang, J. J. Hnilo, M. Fiorino, and G. L. Potter, 2002: NCEP–DOE AMIP-II Reanalysis (R-2). *Bull. Amer. Meteor. Soc.*, **83**, 1631–1644, https://doi.org/10.1175/BAMS-83-11-1631.

Kessler, W. S., 2002: Is ENSO a cycle or a series of events? *Geophys. Res. Lett.*, **29**, 2125, https://doi.org/10.1029/2002GL015924.

Kim, S.-B., T. Lee, and I. Fukumori, 2007: Mechanisms controlling the interannual variations of mixed layer temperature

averaged over the Niño-3 region. *J. Climate*, **20**, 3822–3843, https://doi.org/10.1175/JCLI4206.1.

Kirtman, B. P., and Coauthors, 2014: The North American Multimodel Ensemble: Phase-1 seasonal-to-interannual prediction; Phase-2 toward developing intraseasonal prediction. *Bull. Amer. Meteor. Soc.*, **95**, 585–601, https://doi.org/10.1175/BAMS-D-12-00050.1.

Kleeman, R., J. P. McCreary Jr., and B. A. Klinger, 1999: A mechanism for generating ENSO decadal variability. *Geophys. Res. Lett.*, **26**, 1743–1746, https://doi.org/10.1029/1999GL900352.

Kug, J.-S., F.-F. Jin, and S.-I. An, 2009: Two types of El Niño events: Cold tongue El Niño and warm pool El Niño. *J. Climate*, **22**, 1499–1515, https://doi.org/10.1175/2008JCLI2624.1.

——, J. Choi, S.-I. An, F.-F. Jin, and A. T. Wittenberg, 2010: Warm pool and cold tongue El Niño events as simulated by the GFDL CM2.1 coupled GCM. *J. Climate*, **23**, 1226–1239, https://doi.org/10.1175/2009JCLI3293.1.

Kumar, A., M. Chen, Y. Xue, and D. Behringer, 2015: An analysis of the temporal evaluation of ENSO prediction skill in the context of equatorial Pacific Ocean observing system. *Mon. Wea. Rev.*, **143**, 3204–3213, https://doi.org/10.1175/MWR-D-15-0035.1.

Larson, S. M., and B. P. Kirtman, 2013: The Pacific meridional mode as a trigger for ENSO in a high-resolution coupled model. *Geophys. Res. Lett.*, **40**, 3189–3194, https://doi.org/10.1002/grl.50571.

Latif, M., and Coauthors, 1998: A review of the predictability and prediction of ENSO. *J. Geophys. Res.*, **103**, 14 375–14 393, https://doi.org/10.1029/97JC03413.

Lee, S. K., and G. T. Csanady, 1999: Warm water formation and escape in the upper tropical Atlantic Ocean. 2. A numerical model study. *J. Geophys. Res.*, **104**, 29 573–29 590, https://doi.org/10.1029/1999JC900078.

Lee, T., and M. J. McPhaden, 2010: Increasing intensity of El Niño in the central-equatorial Pacific. *Geophys. Res. Lett.*, **37**, L14603, https://doi.org/10.1029/2010GL044007.

——, I. Fukumori, and B. Tang, 2004: Temperature advection: Internal versus external processes. *J. Phys. Oceanogr.*, **34**, 1936–1944, https://doi.org/10.1175/1520-0485(2004)034<1936:TAIVEP>2.0.CO;2.

Levitus, S., 1982: Climatological Atlas of the World Ocean. NOAA Prof. Paper 13, 173 pp and 17 microfiche.

L'Heureux, M. L., 2018: Overview of the 2017–18 La Niña and El Niño watch in mid-2018. *43rd NOAA Annual Climate Diagnostics and Prediction Workshop*, Santa Barbara, CA, https://doi.org/10.25923/ae2c-v522.

Liu, Z., 1994: A simple model of the mass exchange between the subtropical and tropical ocean. *J. Phys. Oceanogr.*, **24**, 1153–1165, https://doi.org/10.1175/1520-0485(1994)024<1153:ASMOTM>2.0.CO;2.

Lopez, H., and B. Kirtman, 2014: WWBs, ENSO predictability, the spring barrier and extreme events. *J. Geophys. Res. Atmos.*, **119**, 10 114–10 138, https://doi.org/10.1002/2014JD021908.

Lu, P., J. P. McCreary, and B. A. Klinger, 1998: Meridional circulation cells and the source waters of the Pacific Equatorial Undercurrent. *J. Phys. Oceanogr.*, **28**, 62–84, https://doi.org/10.1175/1520-0485(1998)028<0062:MCCATS>2.0.CO;2.

Lu, Q., Z. Ruan, D. P. Wang, D. Chen, and Q. Wu, 2017: Zonal transport from the western boundary and its role in warm water volume changes during ENSO. *J. Phys. Oceanogr.*, **47**, 211–225, https://doi.org/10.1175/JPO-D-16-0112.1.

Luo, J.-J., G. Liu, H. Hendon, O. Alves, and T. Yamagata, 2017: Inter-basin sources for two-year predictability of the multi-year La Niña event in 2010–2012. *Sci. Rep.*, **7**, 2276, https://doi.org/10.1038/s41598-017-01479-9.

McCreary, J. P., and Z. Yu, 1992: Equatorial dynamics in a 2 1/2-layer model. *Prog. Oceanogr.*, **29**, 61–132, https://doi.org/10.1016/0079-6611(92)90003-I.

——, and P. Lu, 1994: Interaction between the subtropical and equatorial ocean circulations: The subtropical cell. *J. Phys. Oceanogr.*, **24**, 466–497, https://doi.org/10.1175/1520-0485(1994)024<0466:IBTSAE>2.0.CO;2.

McPhaden, M. J., 2003: Tropical Pacific Ocean heat content variations and ENSO persistence barriers. *Geophys. Res. Lett.*, **30**, 1480, https://doi.org/10.1029/2003GL016872.

——, 2012: A 21st century shift in the relationship between ENSO SST and warm water volume anomalies. *Geophys. Res. Lett.*, **39**, L09706, https://doi.org/10.1029/2012GL051826.

——, and X. Yu, 1999: Equatorial waves and the 1997-98 El Niño. *Geophys. Res. Lett.*, **26**, 2961–2964, https://doi.org/10.1029/1999GL004901.

——, and D. Zhang, 2002: Slowdown of the meridional overturning circulation in the upper Pacific Ocean. *Nature*, **415**, 603–608, https://doi.org/10.1038/415603a.

——, S. E. Zebiak, and M. H. Glantz, 2006: ENSO as an intriguing concept in Earth science. *Science*, **314**, 1740–1745, https://doi.org/10.1126/science.1132588.

——, T. Lee, and D. McClurg, 2011: El Niño and its relationship to changing background conditions in the tropical Pacific Ocean. *Geophys. Res. Lett.*, **38**, L15709, https://doi.org/10.1029/2011GL048275.

——, A. Santoso, and W. Cai, 2020: *El Niño Southern Oscillation in a Changing Climate. Geophys. Monogr.*, Vol. 253, Amer. Geophys. Union, 528 pp.

Meinen, C. S., and M. J. McPhaden, 2000: Observations of warm water volume changes in the equatorial Pacific and their relationship to El Niño and La Niña. *J. Climate*, **13**, 3551–3559, https://doi.org/10.1175/1520-0442(2000)013<3551:OOWWVC>2.0.CO;2.

Neske, S., and S. McGregor, 2018: Understanding the warm water volume precursor of ENSO events and its interdecadal variation. *Geophys. Res. Lett.*, **45**, 1577–1585, https://doi.org/10.1002/2017GL076439.

——, ——, M. Zeller, and D. Dommenget, 2021: Wind spatial structure triggers ENSO's oceanic warm water volume changes. *J. Climate*, **34**, 1985–1999, https://doi.org/10.1175/JCLI-D-20-0040.1.

Okumura, Y. M., and C. Deser, 2010: Asymmetry in the duration of El Niño and La Niña. *J. Climate*, **23**, 5826–5843, https://doi.org/10.1175/2010JCLI3592.1.

——, M. Ohba, C. Deser, and H. Ueda, 2011: A proposed mechanism for the asymmetric duration of El Niño and La Niña. *J. Climate*, **24**, 3822–3829, https://doi.org/10.1175/2011JCLI3999.1.

Paek, H., J.-Y. Yu, and C. Qian, 2017: Why were the 2015/2016 and 1997/1998 extreme El Niños different? *Geophys. Res. Lett.*, **44**, 1848–1856, https://doi.org/10.1002/2016GL071515.

Park, J.-H., S.-I. An, J.-S. Kug, Y.-M. Yang, T. Li, and H.-S. Jo, 2020: Mid-latitude leading double-dip La Niña. *Int. J. Climatol.*, **41**, E1353–E1370, https://doi.org/10.1002/joc.6772.

Planton, Y., J. Vialard, E. Guilyardi, M. Lengaigne, and T. Izumo, 2018: Western Pacific oceanic heat content: A better predictor of La Niña than of El Niño. *Geophys. Res. Lett.*, **45**, 9824–9833, https://doi.org/10.1029/2018GL079341.

Puy, M., and Coauthors, 2019: Influence of westerly wind events stochasticity on El Niño amplitude: The case of 2014 vs. 2015. *Climate Dyn.*, **52**, 7435–7454, https://doi.org/10.1007/s00382-017-3938-9.

Ren, H.-L., and F.-F. Jin, 2013: Recharge oscillator mechanisms in two types of ENSO. *J. Climate*, **26**, 6506–6523, https://doi.org/10.1175/JCLI-D-12-00601.1.

Reynolds, R. W., N. A. Rayner, T. M. Smith, D. C. Stokes, and W. Wang, 2002: An improved in situ and satellite SST analysis for climate. *J. Climate*, **15**, 1609–1625, https://doi.org/10.1175/1520-0442(2002)015<1609:AIISAS>2.0.CO;2.

Schopf, P. S., and M. A. Cane, 1983: On equatorial dynamics, mixed layer physics, and sea surface temperature. *J. Phys. Oceanogr.*, **13**, 917–935, https://doi.org/10.1175/1520-0485(1983)013<0917:OEDMLP>2.0.CO;2.

Schott, F. A., J. P. McCreary, and G. C. Johnson, 2004: Shallow overturning circulations of the tropical–subtropical oceans. *Earth's Climate: The Ocean–Atmosphere Interaction. Geophys. Monogr.*, Vol. 147, Amer. Geophys. Union, 261–304.

Su, J., B. Xiang, B. Wang, and T. Li, 2014: Abrupt termination of the 2012 Pacific warming and its implication on ENSO prediction. *Geophys. Res. Lett.*, **41**, 9058–9064, https://doi.org/10.1002/2014GL062380.

Suarez, M. J., and P. S. Schopf, 1988: A delayed action oscillator for ENSO. *J. Atmos. Sci.*, **45**, 3283–3287, https://doi.org/10.1175/1520-0469(1988)045<3283:ADAOFE>2.0.CO;2.

Timmermann, A., and Coauthors, 2018: El Niño–Southern Oscillation complexity. *Nature*, **559**, 535–545, https://doi.org/10.1038/s41586-018-0252-6.

Toyoda, T., Y. Fujii, T. Yasuda, N. Usui, T. Iwao, T. Kuragano, and M. Kamachi, 2013: Improved analysis of seasonal-interannual fields using a global ocean data assimilation system. *Theor. Appl. Mech. Japan*, **61**, 31–48, https://doi.org/10.11345/nctam.61.31.

Vernieres, G., C. Keppenne, M. M. Rienecker, J. Jacob, and R. Kovach, 2012: The GEOS-ODAS: Description and evaluation. NASA Tech. Rep. Series on Global Modeling and Data Assimilation, NASA/TM-2012-104606, Vol. 30, 60 pp.

Vimont, D. J., J. M. Wallace, and D. S. Battisti, 2003: The seasonal footprinting mechanism in the Pacific: Implications for ENSO. *J. Climate*, **16**, 2668–2675, https://doi.org/10.1175/1520-0442(2003)016<2668:TSFMIT>2.0.CO;2.

Wang, J., Y. Lu, F. Wang, and R. H. Zhang, 2017: Surface current in "hotspot" serves as a new and effective precursor for El Niño prediction. *Sci. Rep.*, **7**, 166, https://doi.org/10.1038/s41598-017-00244-2.

Wang, W., M. Chen, and A. Kumar, 2010: An assessment of the CFS real-time seasonal forecasts. *Wea. Forecasting*, **25**, 950–969, https://doi.org/10.1175/2010WAF2222345.1.

Wen, C., P. Chang, and R. Saravanan, 2010: Effect of Atlantic meridional overturning circulation changes on tropical Atlantic sea surface temperature variability: A 2 1/2-layer reduced-gravity ocean model study. *J. Climate*, **23**, 312–332, https://doi.org/10.1175/2009JCLI3042.1.

——, A. Kumar, Y. Xue, and M. J. McPhaden, 2014: Changes in tropical Pacific thermocline depth and their relationship to ENSO after 1999. *J. Climate*, **27**, 7230–7249, https://doi.org/10.1175/JCLI-D-13-00518.1.

Wu, X., Y. M. Okumura, and P. N. DiNezio, 2019: What controls the duration of El Niño and La Niña events? *J. Climate*, **32**, 5941–5965, https://doi.org/10.1175/JCLI-D-18-0681.1.

Xiang, B., B. Wang, and T. Li, 2013: A new paradigm for the predominance of standing central Pacific warming after the late 1990s. *Climate Dyn.*, **41**, 327–340, https://doi.org/10.1007/s00382-012-1427-8.

Xue, Y., M. Chen, A. Kumar, Z.-Z. Hu, and W. Wang, 2013: Prediction skill and bias of tropical Pacific sea surface temperatures in the NCEP Climate Forecast System version 2. *J. Climate*, **26**, 5358–5378, https://doi.org/10.1175/JCLI-D-12-00600.1.

——, and Coauthors, 2017: A real-time ocean reanalyses intercomparison project in the context of tropical Pacific observing system and ENSO monitoring. *Climate Dyn.*, **49**, 3647–3672, https://doi.org/10.1007/s00382-017-3535-y.

Yin, Y., O. Alves, and P. R. Oke, 2011: An ensemble ocean data assimilation system for seasonal prediction. *Mon. Wea. Rev.*, **139**, 786–808, https://doi.org/10.1175/2010MWR3419.1.

You, Y., and J. C. Furtado, 2017: The role of South Pacific atmospheric variability in the development of different types of ENSO. *Geophys. Res. Lett.*, **44**, 7438–7446, https://doi.org/10.1002/2017GL073475.

Yu, J.-Y., and S. T. Kim, 2010: Three evolution patterns of central-Pacific El Niño. *Geophys. Res. Lett.*, **37**, L08706, https://doi.org/10.1029/2010GL042810.

——, and S.-W. Fang, 2018: The distinct contributions of the seasonal footprinting and charged-discharged mechanisms to ENSO complexity. *Geophys. Res. Lett.*, **45**, 6611–6618, https://doi.org/10.1029/2018GL077664.

——, H.-Y. Kao, and T. Lee, 2010: Subtropics-related interannual sea surface temperature variability in the equatorial central Pacific. *J. Climate*, **23**, 2869–2884, https://doi.org/10.1175/2010JCLI3171.1.

Zebiak, S. E., 1989: Ocean heat content variability and El Niño cycles. *J. Phys. Oceanogr.*, **19**, 475–486, https://doi.org/10.1175/1520-0485(1989)019<0475:OHCVAE>2.0.CO;2.

Zhang, C., and J. Gottschalck, 2002: SST anomalies of ENSO and the Madden–Julian oscillation in the equatorial Pacific. *J. Climate*, **15**, 2429–2445, https://doi.org/10.1175/1520-0442(2002)015<2429:SAOEAT>2.0.CO;2.

Zhang, R.-H., F. Zheng, J. Zhu, and Z. Wang, 2013: A successful real-time forecast of the 2010–11 La Niña event. *Sci. Rep.*, **3**, 1108, https://doi.org/10.1038/srep01108.

Zhang, S., M. J. Harrison, A. Rosati, and A. Wittenberg, 2007: System design and evaluation of coupled ensemble data assimilation for global oceanic climate studies. *Mon. Wea. Rev.*, **135**, 3541–3564, https://doi.org/10.1175/MWR3466.1.

Zhang, X., and M. J. McPhaden, 2010: Surface layer heat balance in the eastern equatorial Pacific Ocean on interannual time scales: Influence of local versus remote wind forcing. *J. Climate*, **23**, 4375–4394, https://doi.org/10.1175/2010JCLI3469.1.

Zuo, H., M. A. Balmaseda, K. Mogensen, and S. Tietsche, 2018: OCEAN5: The ECMWF ocean reanalysis system and its real-time analysis component. ECMWF Tech. Memo. 823, 44 pp., https://doi.org/https://doi.org/10.21957/la2v0442.